AGU PUBLICATIONS

JGR

Journal of Geophysical Research: Earth Surface

RESEARCH ARTICLE
10.1002/2015JF003671

Key Points:
- Bayesian network used to identify correlations between morphological variables for a barrier island
- Short- and large-scale morphological metrics correspond to shoreline change and coastal management
- Skillful prediction of dune height, beach width, and beach height useful to assess future conditions

Supporting Information:
- Table S1 and Data Set S1 caption
- Data Set S1

Correspondence to:
B. T. Gutierrez,
bgutierrez@usgs.gov

Citation:
Gutierrez, B. T., N. G. Plant, E. R. Thieler, and A. Turecek (2015), Using a Bayesian network to predict barrier island geomorphologic characteristics, *J. Geophys. Res. Earth Surf.*, *120*, 2452–2475, doi:10.1002/2015JF003671.

Received 17 JUL 2015
Accepted 8 NOV 2015
Accepted article online 12 NOV 2015
Published online 4 DEC 2015

Using a Bayesian network to predict barrier island geomorphologic characteristics

Benjamin T. Gutierrez[1], Nathaniel G. Plant[2], E. Robert Thieler[1], and Aaron Turecek[3]

[1]U.S. Geological Survey, Woods Hole, Massachusetts, USA, [2]U.S. Geological Survey, St. Petersburg, Florida, USA, [3]Now at Real Time Research, Inc., Bend, Oregon, USA

Abstract Quantifying geomorphic variability of coastal environments is important for understanding and describing the vulnerability of coastal topography, infrastructure, and ecosystems to future storms and sea level rise. Here we use a Bayesian network (BN) to test the importance of multiple interactions between barrier island geomorphic variables. This approach models complex interactions and handles uncertainty, which is intrinsic to future sea level rise, storminess, or anthropogenic processes (e.g., beach nourishment and other forms of coastal management). The BN was developed and tested at Assateague Island, Maryland/Virginia, USA, a barrier island with sufficient geomorphic and temporal variability to evaluate our approach. We tested the ability to predict dune height, beach width, and beach height variables using inputs that included longer-term, larger-scale, or external variables (historical shoreline change rates, distances to inlets, barrier width, mean barrier elevation, and anthropogenic modification). Data sets from three different years spanning nearly a decade sampled substantial temporal variability and serve as a proxy for analysis of future conditions. We show that distinct geomorphic conditions are associated with different long-term shoreline change rates and that the most skillful predictions of dune height, beach width, and beach height depend on including multiple input variables simultaneously. The predictive relationships are robust to variations in the amount of input data and to variations in model complexity. The resulting model can be used to evaluate scenarios related to coastal management plans and/or future scenarios where shoreline change rates may differ from those observed historically.

1. Introduction

Barrier islands are constantly evolving coastal landforms where nearshore currents driven by winds, waves, and tides actively shape the islands (see reviews in *Davis* [1994] and *FitzGerald et al.* [2008]). Over short timescales (days to months), storms modify the barrier island landscape through erosion [*Morton et al.*, 1994; *Zhang et al.*, 2002; *List et al.*, 2006], overwash [*Sallenger*, 2000; *Morton and Sallenger*, 2003; *Stockdon et al.*, 2007; *Roelvink et al.*, 2009; *Plant and Stockdon*, 2012], and episodic inlet formation [*Leatherman*, 1983; *Davis*, 1994; *Moslow and Heron*, 1994; *FitzGerald et al.*, 2008; *Sherwood et al.*, 2014]. Over longer timescales spanning decades to centuries, sea level rise increases the potential of storms to drive the evolution of the barrier island system [*FitzGerald et al.*, 2008; *Gutierrez et al.*, 2009]. With increased potential for future sea level rise and for increased frequency of storm-related overwash, many barrier islands are expected to evolve at a faster pace than what has been observed during the late Holocene and historically [*Gutierrez et al.*, 2007, 2009; *FitzGerald et al.*, 2008].

The ability to predict barrier island vulnerability to storm-induced erosion that is coupled to longer-term morphological evolution due to sea level rise can be used to guide decisions to avoid, mitigate, or adapt coastal ecosystems and human development in the future [*Climate Change Science Program*, 2009; *Melillo et al.*, 2014]. For instance, management practices may include beach nourishment or berm and dune building, which affects the response to storms and alters habitat [*Schupp et al.*, 2013]. More broadly, barrier islands are present along 6% of the world's shoreline [*Stutz and Pilkey*, 2011]; they comprise a large portion of the U.S. coast [*Morton et al.*, 2004; *Morton and Miller*, 2005; *Hapke et al.*, 2011]. Barrier islands also provide important ecologic and economic benefits through tourism and recreation and by sheltering wetlands, estuaries, and the mainland from the open ocean [*Stone and McBride*, 1998; *Stone et al.*, 2005; *Day et al.*, 2007]. Consequently, decisions regarding mitigation or adaptation to evolving barrier islands have a variety of potentially competing objectives that need to be addressed quantitatively [*Tribbia and Moser*, 2008]. Moreover, the factors affecting barrier island vulnerability need to be evaluated statistically, due to inherent uncertainty in climate and geomorphic processes [*Cowell et al.*, 2006].

A variety of approaches have been used to examine storm and sea level rise impacts on coastal regions. These methods range from simple inundation mapping (i.e., the "bathtub" approach) [*Najjar et al*., 2000; *Titus and Richman*, 2001; *Kirshen et al*., 2008; *Cooper et al*., 2008; *Gesch et al*., 2009; *Weiss et al*., 2011; *Strauss et al*., 2012] to models that evaluate the dynamic response of coastal landforms such as barrier islands [*Cowell et al*., 1995; *Stolper et al*., 2005; *McNamara et al*., 2011; *Corbella and Stretch*, 2012; *Roelvink et al*., 2009; *McCall et al*., 2010; *Lindemer et al*., 2010; *Lorenzo-Trueba and Ashton*, 2014; *Sherwood et al*., 2014]. While the most detailed numerical models for predicting barrier island response to storms have excellent skill for specific events such as nor'easters and hurricanes [*Roelvink et al*., 2009; *McCall et al*., 2010, *Lindemer et al*., 2010], these models have not been used to make longer-term predictions that would simulate evolution in response to multiple storms and changes in sea level. For long-term simulations, simplified morphodynamic models have been useful to explore the sensitivity of barrier island evolution to sea level rise, storminess, and geological constraints [*Cowell et al*., 1995; *Stolper et al*., 2005; *McNamara and Werner*, 2008a, 2008b; *Moore et al*., 2010; *Lorenzo-Trueba and Ashton*, 2014].

Another approach that includes some overlap with both inundation mapping and detailed numerical modeling is to develop a model based on observed geomorphic metrics that represent the actual impacts of short- and long-term processes on barrier islands. The metrics capture the likelihood of erosion, overwash, and inlet formation that occur on short timescales, as well as longer-term changes in barrier island geometry and position. *Sallenger* [2000] and *Stockdon et al*. [2007, 2009] developed an approach to evaluate the vulnerability of barrier islands to storms. In particular, they showed that dune crest height is an important parameter for identifying barrier island vulnerability to maximum water level elevations caused by a combination of storm surge and wave runup during storms [*Stockdon et al*., 2007]. Others have shown that dune height is not the only important morphological characteristic that determines storm vulnerability. For example, beach width and dune width have also been shown to control the severity of erosion during storms [*Thieler and Young*, 1991; *Claudino-Sales et al*., 2008; *Plant and Stockdon*, 2012]. Barrier island width and height above sea level are also relevant for application to future sea level scenarios, including groundwater system response to sea level rise [*Masterson et al*., 2013]. Finally, long-term shoreline change is correlated to sea level rise [*Gutierrez et al*., 2011; *Romine et al*., 2013], and these long-term processes act as drivers of change in the other geomorphic features including marshes, inlets, and the cross-shore profile [*FitzGerald et al*., 2008; *Passeri et al*., 2015]. Additionally, anthropogenic modification such as dune building and beach nourishment can directly affect long-term or short-term variability [*Slott et al*., 2010; *Magliocca et al*., 2011; *Ells and Murray*, 2012; *Hapke et al*., 2013; *Schupp et al*., 2013; *Van Den Hoek et al*., 2012; *Plant et al*., 2014].

We approach the problem of predicting future barrier island characteristics that couple short-term and long-term processes with a Bayesian network (BN) [*Charniak*, 1991; *Cooper and Herskovits*, 1992; *Marcot et al*., 2006; *Wikle and Berliner*, 2007] that statistically couples physical attributes of a barrier island derived from coastal lidar data sets, long-term shoreline change rates based on imagery and lidar, and records of anthropogenic modifications of a barrier island geomorphic setting. A key utility of the BN is that it captures the uncertainty in the relationships between the geomorphic variables, and it can be driven with uncertainty in the inputs. For example, the BN handles uncertainty in future estimates of both the climate and anthropogenic drivers.

BNs have been used in a number of recent studies to evaluate the probabilities of shoreline change or morphological changes given knowledge of forcing, boundary, or other morphological conditions [*Plant and Holland*, 2011; *Gutierrez et al*., 2011; *Lentz and Hapke*, 2011; *Hapke et al*., 2013; *Plant and Stockdon*, 2012; *Plant et al*., 2014]. We use data from Assateague Island, a largely undeveloped barrier island along the Maryland and Virginia coast of the United States, to develop and test the model. This island has substantial diversity in dune height and beach width, and we assume that spatial variations in these relatively short-scale features are correlated to large-scale variations in island width, shoreline change rates, and degree of anthropogenic modifications (e.g., beach nourishment). Thus, we expect that the island can be used to test predictions from a BN that represent both short and long spatial scales. Although we utilize data from several different time periods, we are not explicitly testing a time-resolving model that could include short-term variations in the morphologic drivers (i.e., individual storms). Instead, we are seeking the set of morphologic states that are admissible through a range of short-term transitions captured by our data. In this sense, the drivers are assumed to be constant over the short term and are represented by the two long-term forcing terms (shoreline change rate and anthropogenic modifications), which vary along

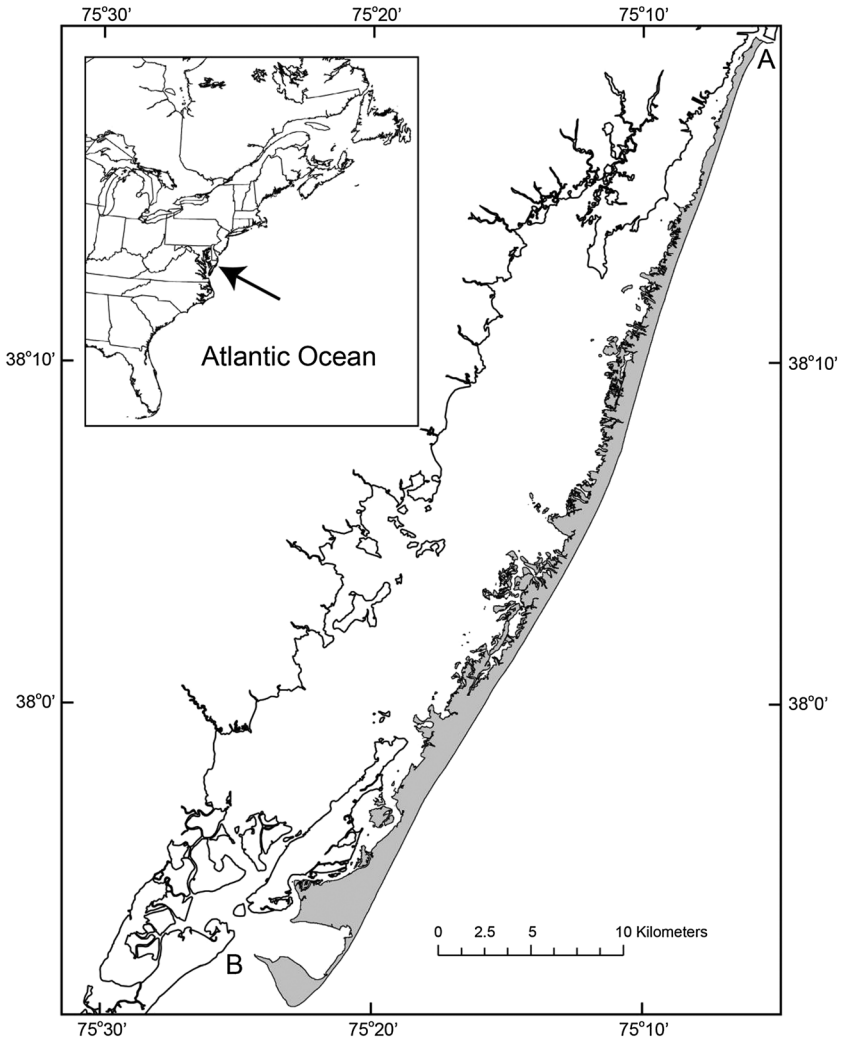

Figure 1. Location map showing Assateague Island, highlighted in gray, along the mid-Atlantic coast of the United States. Letters mark Ocean City inlet (A) and Chincoteague inlet (B).

the shoreline of Assateague Island. Our assumption extends to the details of sediment transport, which are captured in the long-term shoreline change rate (e.g., representing sediment transport convergences and divergences), while short-term changes (e.g., overwash fluxes coupled to dune heights) are captured statistically. Ideally, the model extracts properties that represent climatological averages at multiple scales.

The following sections describe the study site in detail and how our BN was developed to predict specific geomorphic characteristics that describe barrier island morphology and vulnerability. The robustness of these predictions is tested. Then we identify the complex correlations between the geomorphic variables and evaluate the BN prediction skill, describe the implications of the predictability of morphologic features and the residual uncertainty, evaluate our assumptions, and explore different prediction scenarios.

2. Study Site

Assateague Island is located along the mid-Atlantic coast of the eastern United States, between Ocean City, Maryland to the north, and Chincoteague, Virginia, to the south (Figure 1). This midlatitude, wave-dominated, microtidal barrier island [*Hayes*, 1979] is approximately 60 km long and varies in width from approximately 220 m along portions of its northern end to nearly 4.5 km near Chincoteague. The island is generally low lying, with a mean elevation of 0.9 m (NAVD88). There are forested dune ridges in several portions of the island

with maximum elevations ranging from 5 to 15 m, with the highest elevations toward the southern end of the island.

Prior to 1933, Assateague Island was part of Fenwick Island to the north and extended the length of Delaware and Maryland's coast south to Chincoteague [*Dean and Perlin*, 1979; *Dolan et al*., 1980; *Krantz et al*., 2009]. In 1933, a hurricane cut an inlet at Ocean City, Maryland. The inlet was made permanent by the addition of riprap jetties in 1934 and breakwaters along the southern channel of the inlet in the subsequent years. The presence of the jetties interrupted the net southward alongshore transport of sand due to impoundment of sand on the north jetty (the beach is noticeably wider even today) and the development of a large ebb tidal delta offshore of Ocean City inlet. Consequently, the northern 10 km of Assateague Island experienced rapid erosion, with the barrier retreating several hundred meters landward (see review in *Dean and Perlin* [1977], *Dolan et al*. [1980], and *Krantz et al*. [2009]). Large storms during the mid-1950s and early 1960s produced breaches on northern Assateague Island that resulted in the artificial placement of dredged sediment to return the barrier to its prestorm state. Since that time, a number of other anthropogenic modifications have been required to maintain the inlet and the integrity of northern Assateague Island. Initially, this involved mechanical sand bypassing that used sediment dredged from Ocean City inlet and its ebb tidal delta and placed this material in the surf zone of northern Assateague Island, 5–8 km to the south. In addition, emergency storm berms were built in the same region to reduce significant overwash during the late 1990s [*Schupp et al*., 2013]. Large storms have overwashed portions of Assateague Island episodically, leading to dune erosion and in some cases creating temporary inlets [*Truitt*, 1968; *Krantz et al*., 2009]. Most recently, storms such as Nor'Ida [*NOAA*, 2009; *U.S. Geological Survey* (*USGS*), 2009], Hurricane Irene [*NOAA*, 2011; *USGS*, 2011], and Hurricane Sandy [*USGS*, 2012] have generated high storm surges and wave runup that led to overwash at several locations on the island.

3. Methods

We hypothesize that a basic set of morphological characteristics, such as dune crest height (DH), beach width (BW), and/or beach height (BH), can be predicted from longer-term, larger-scale attributes such as the rate of historical shoreline change or distance to the nearest tidal inlet. We express this relationship in the form

$$[\mathrm{DH}(\vec{x}), \mathrm{BH}(\vec{x}), \mathrm{BW}(\vec{x})] = \mathrm{funct.}[\mathrm{DI}(\vec{x}), \mathrm{SLC}(\vec{x}),\ \mathrm{ME}(\vec{x}), \mathrm{WB}(\vec{x}), \mathrm{AM}(\vec{x})] \tag{1}$$

where DH, BH, and BW describe the short-scale geomorphology evaluated on a cross-island transect and are indexed to a spatial location vector $\vec{x}$ (i.e., latitude and longitude). Large-scale, long-term, and external forcing variables include distance to nearest inlet (DI), the long-term shoreline change rate (SLC), anthropogenic modification applied at each location (AM), the mean elevation of a barrier cross section (ME), and barrier width (WB). These variables have been shown to be important to storm [*Stockdon et al*., 2007; *Plant et al*., 2012] and habitat vulnerability assessments [*Gieder et al*., 2014]. Our goal is to formulate this model in the form of a BN.

3.1. Bayesian Network Framework

To construct a BN that can test our hypothesis, we cast equation (1) as a probabilistic relationship

$$p(\mathrm{DH}, \mathrm{BH}, \mathrm{BW}|\mathrm{DI}, \mathrm{SLC}, \mathrm{ME}, \mathrm{WB}, \mathrm{AM}) = \mathrm{funct.}[p(\mathrm{DH}, \mathrm{BH}, \mathrm{BW}, \mathrm{DI}, \mathrm{SLC}, \mathrm{ME}, \mathrm{WB}, \mathrm{AM})] \tag{2}$$

The variables targeted for prediction also occur as input, because BNs include prior knowledge of each variable; thus, equation (2) can be modeled with BNs. BNs are directed acyclic graphs that apply Bayes' theorem to relate the probability of an event R given the occurrence of another event O [*Jensen and Nielsen*, 2007]:

$$p(R_i|O_j) = \frac{p(O_j|R_i) \cdot p(R_i)}{P(O_j)} \tag{3}$$

where the "events" in our case will be particular combinations of geomorphic variables. In equation (3), the left side denotes the conditional probability of a response variable R_i (i.e., BW, BH, or DH) given a corresponding set of input observations O_j (i.e., any or all of the variables, where the subscript j could represent the specific inputs at each location as well an index to our set of test scenarios). The subscript i represents a particular spatial location, which we define as data along a transect that cuts across the island perpendicular to the shoreline.

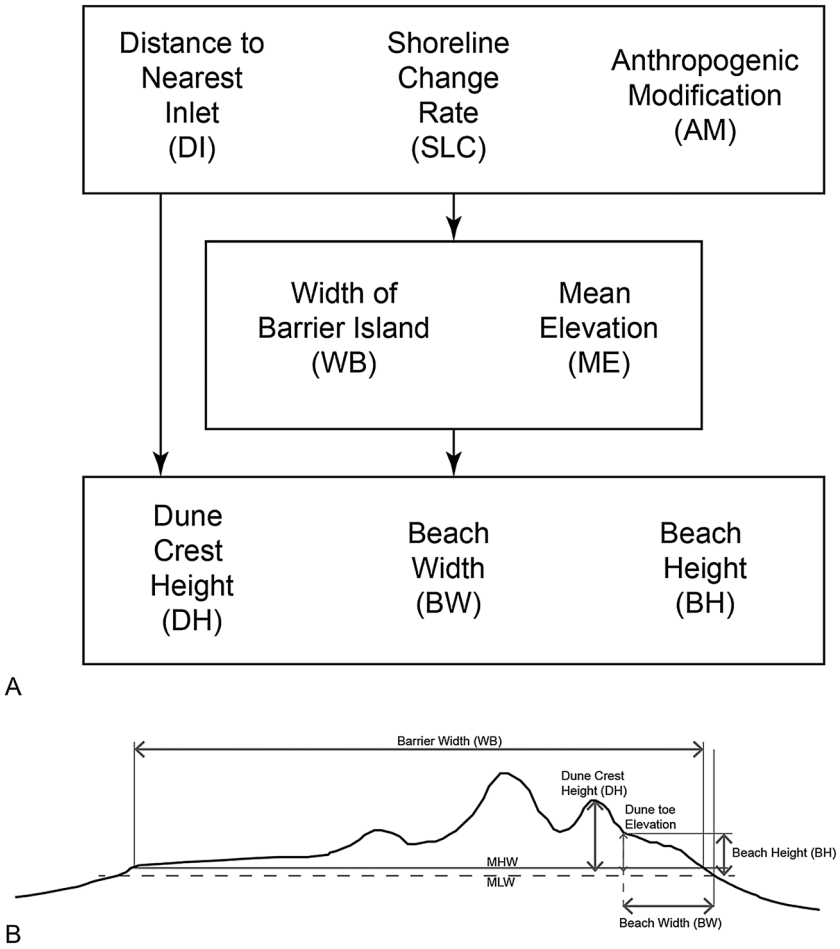

Figure 2. Schematic diagrams showing (a) the general structure of the Bayesian network that was developed and implemented for this study and (b) the barrier island cross section illustrating four of the barrier island metrics utilized in the Bayesian network: dune crest height (DH), beach height (BH), beach width (BW), and barrier width (WB). MHW = local mean high water, MLW = local mean low water. Dune toe elevation is shown here because it is a reference point used to calculate beach width and beach height.

The first term of the numerator is known as the likelihood and is the probability of the observation given that the response is known. This term provides a measure of the correlation between observation and response. The second term in the numerator is the prior probability of the response, and it is the probability of a particular response integrated over all observations. Lastly, the denominator is a normalization factor to account for the likelihood of the particular set of observations.

We used the Netica software package (Norsys, Netica, v. 4.16, www.norsys.com) to build a BN representing equation (2) in the form of equation (3) (Figure 2a). In a BN, each variable is represented by a node that stores the probabilities of occurrence of a variable conditioned on the value of its parent variables. The arrows in Figure 2a indicate parent-child relationships. A node with no parents stores only the prior probabilities. There are multiple connections between each variable because each geomorphic characteristic is believed to influence each of the others; hence, the BN is fully connected such that variables within each of the three forcing and scale groups are correlated to each other as well as to variables in other groups. The forcing variables (SLC, DI, and AM) are parents to large scale (WB and ME), and the large scale is the parent of the shorter scales (DH, BW, and BH). Although the arrows point in one direction, this only indicates an imposed parent-child hierarchy representing a morphologic feedback loop where the child variables can ultimately influence the parents (e.g., after many storm events or after a long period of sea level rise). In the BN, the correlations can be applied in either direction. The probabilities are stored in discrete tables called conditional probability tables (CPTs) that require each variable to be divided into finite bin ranges. The CPTs for most nodes

Table 1. Summary of Variables Included the BN, With an Explanation of the Discretization That Was Applied to Each Node in the BN

Variable	Number of Real Values	Binned Values					
		1	2	3	4	5	6
Shoreline change (m/yr)	3,143	< -1.0	-1.0–0	0–1.0	>1.0	-	-
Anthropogenic modification	3,143	None/minimal	Construction present	Occasional modification	Construction plus occasional restoration	Ongoing restoration	Ongoing restoration plus construction
Dune crest height (m)	2,125	<2.0	2.0–3.0	3.0–4.0	4.0–5.0	>5.0	-
Island width (m)	3,143	100–700	700–1,100	1,100–1,500	1,500–3,500	-	-
Beach width (m)	2,070	<50	50–75	75–100	100–150	150–600	
Beach height (m)	1,357	<2.5	2.5–3.0	3.0–3.5	3.5–4.0	4.0–5.7	-
Mean barrier profile elevation (m)	1,836	0.25–0.75	0.75–1.0	1.0–1.25	1.25–5.9	-	-
Distance to nearest inlet (m)	3,143	0–10,000	10,000–17,000	17,000–24,000	24,000–33,000	-	-

were discretized into four or five bins (Table 1). Bin widths were determined by subjectively balancing the need to have enough bins to resolve meaningful scenarios and thresholds but not exceeding the limits imposed by data accuracy and resolution or exceeding a level of model complexity that degrades the predictive robustness. For the AM node, the data were discrete, consisting of six states corresponding to combinations of management scenarios.

To implement a BN, CPT values must be learned from data, other models, or even expert opinion. In this paper we refer to the process of estimating the CPT tables via importing our data sets as "training." Training depends on both the selection of one or more data sets and on the method used to estimate CPT tables. We used the expectation maximization approach [*Lauritzen*, 1995]. Once trained, the BN can be used to make probabilistic predictions. In the following sections, we describe the data sets used for training and testing; we describe methods for evaluating the robustness of predictive skill; and we describe how the BN is used to conduct analysis, including sensitivity of predictions to variations in the input as well as for forecasting, scenarios where we impose generalized conditions on the input to assess the impact of variations in shoreline erosion rates and anthropogenic modifications.

3.2. Data Sources and Extraction of Variables

Data describing the eight model variables were extracted along 1171 cross-island transects spaced at 50 m intervals alongshore. Ideally, all variables are available at all locations. However, one of the advantages of the BN approach is that incomplete data are tolerated. Transects matched those used to estimate a long-term historical shoreline change rate at Assateague Island [*Himmelstoss et al*., 2010]. In a few instances, additional transects were added to fill gaps where shoreline change transects were missing. Lidar metrics, described in detail below and illustrated in Figure 2b, were obtained by applying methods described in *Stockdon et al*. [2009] to three lidar data sets acquired by the U.S. Geological Survey in 1999, 2002, and 2008 (data used from 1999 and 2002 datasets provided in supporting information, *Bonisteel et al*. [2009]). These three lidar data sets were chosen because they cover the majority of the barrier island and span a range of geomorphic conditions. The 1999 data set was collected a year after major overwash occurred in February 1998 on the north end of the barrier island. The 2002 lidar data set was collected prior to a major beach nourishment effort and documents the barrier island geomorphology 4 years after the 1998 overwash event. The 2008 data set is representative of a barrier island that has been subject to erosion mitigation efforts and relatively unaffected by overwash for the 5 years preceding the acquisition of this data set. Eight variables (Figure 3) are extracted from the lidar data, aerial imagery, or derived from existing analyses.

1. *Dune height* (DH) influences whether a barrier island is eroded, overwashed, or inundated by storm surge and wave runup *Sallenger* [2000]. In this study, DH is the elevation of the foredune crest as defined in *Stockdon et al*. [2007, 2009, 2012]. DH elevations are referenced to the NAVD88 datum.

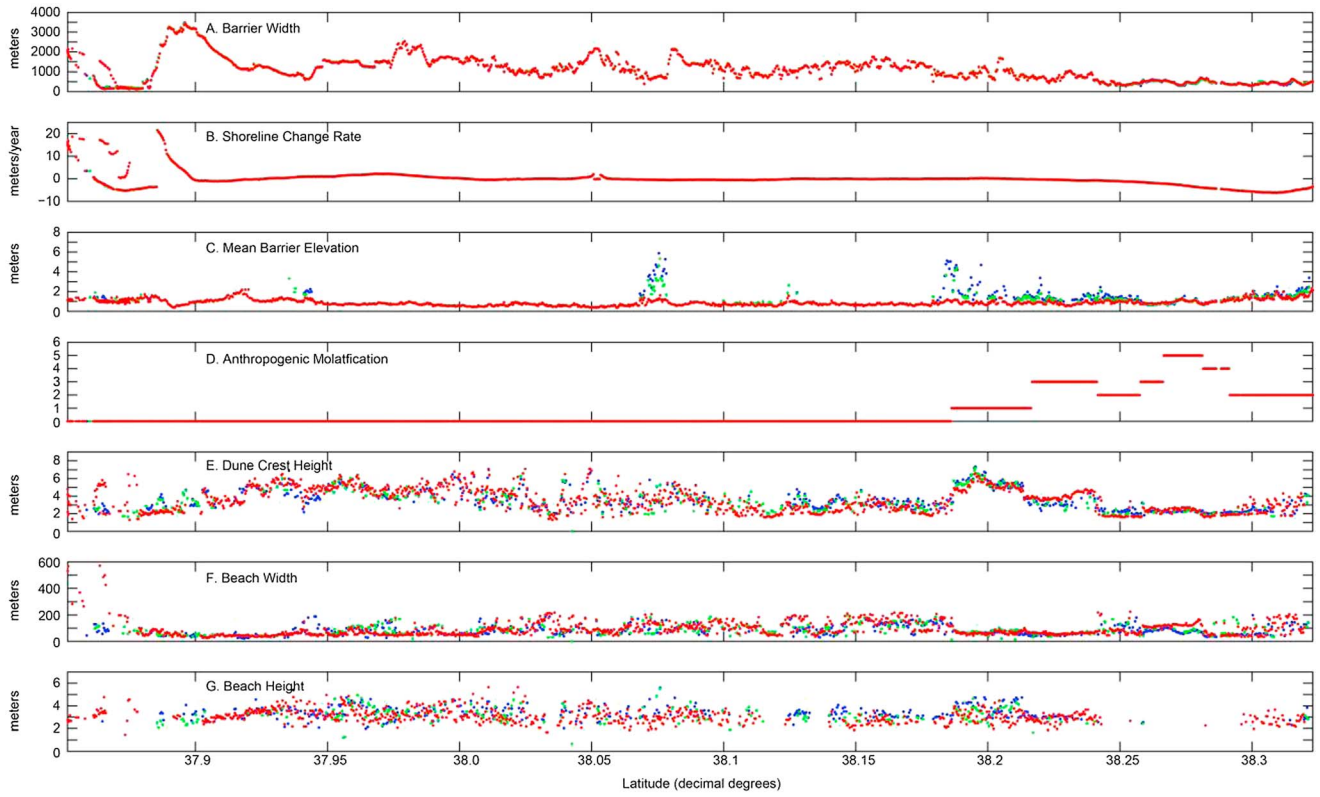

Figure 3. Spatial distribution of input data used in this study. Colored markers depict data from 1999 (blue), 2002 (green), and 2008 (red). Figure 3d, displaying anthropogenic modifications, is coded according to definitions presented in section 3.2.

2. *Beach width* (BW) was calculated as the horizontal distance between the dune toe location [*Stockdon et al*., 2009] and the location of the mean low water (MLW) elevation along a transect. The local MLW elevation is −0.66 m relative to the NAVD88 datum [*Weber et al*., 2005; *National Ocean Service*, 2011] (Ocean City pier station: 0570280).
3. *Beach height* (BH), in combination with beach width, can be used to compute beach volume and has an influence on beach vegetation and shorebird nesting [*Gieder et al*., 2014]. Here BH is defined as the difference between the dune toe elevation and the local MLW elevation (−0.66 m NAVD88).
4. *Distance to nearest inlet* (DI) was computed as alongshore distance of each sampling transect from the nearest tidal inlet, either Ocean City or Chincoteague inlet (Figure 1). This distance includes changes in the path of the shoreline rather than just a straight-line distance between each transect and the inlet and reflects sediment transport pathways.
5. *Long-term shoreline change rates* (SLC) were obtained from the U.S. Geological Survey National Assessment of Shoreline Change [*Hapke and Plant*, 2010; *Himmelstoss et al*., 2010] analysis, which represents changes over the past ~150 years. We used the linear regression rates of long-term shoreline change calculated from a set of 6–10 historical shorelines spanning 1845–2000.
6. *Anthropogenic modifications* (AM) were quantified by classifying infrastructure, such as paved roads and buildings, shoreline engineering, and nourishment occurring over the last 30–40 years (i.e., since 1970). Sources of information include *Morton et al*. [2007], *Krantz et al*. [2009], and geographic information system data sets available from the National Park Service and by inspection of aerial photographs. The classification includes six discrete states:
   a. *None* specifies the absence of shoreline engineering practices such as beach nourishment, berm or dune construction, and infrastructure such as paved roads, parking lots, or buildings.
   b. *Construction present* indicates the presence of parking lots, paved roads, buildings, or constructed berms or buildings.

c. *Occasional modification* indicates that beach (or offshore) nourishment has been undertaken at least once since 1970.
d. *Construction plus occasional modification* indicates that both b and c are true on a transect.
e. *Ongoing modification* indicates that nourishment (e.g., sand added to the surf zone) has been undertaken on a sustained basis at any time since 1970.
f. *Ongoing modification plus construction* indicates that b or e is true on a transect.

7. *Mean barrier elevation* (ME) was defined by averaging elevations within 5 m bins along each barrier-normal transect (e.g., Figure 2b) and then taking a mean value for each transect. The averaging process filtered short-scale features and observational noise. The 1999 and 2002 data sets contained numerous outlier elevations in the interior portions of the barrier that were removed prior to averaging. Mean barrier elevations were calculated for only those transects having less than 20% missing values within the 5 m bins. Locations not satisfying this criterion were marked as missing.
8. *Barrier island width* (WB) was calculated as the distance between the back-barrier and seaward MHW shorelines, using 2008 lidar data and a back-barrier shoreline derived from imagery. To develop a MWH contour, lidar elevation values were adjusted to local MHW using NOAA's VDatum software [*Yang et al.*, 2008] and the zero-elevation contour was interpolated along the back-barrier regions. WB only included regions of the barrier above the MHW level and did not extend into any of the sinuous or intervening back-barrier waterways and islands. Large portions of the 1999 and 2002 lidar data sets did not extend to the back-barrier shoreline regions of Assateague Island. To generate estuarine shorelines for these years, we used the 2008 back-barrier shoreline as a starting point and modified the shorelines using aerial photos from 1999 and 2002 and a National Park Service shoreline that was generated from data collected in 2003.

3.3. Bayesian Network Skill Assessment

Before using a trained BN for analysis, such as sensitivity studies and forecasting, we must evaluate its predictive skill. The training requires estimating the values of a large number of conditional probabilities (about 240,000 values). Many of these values are zero, or nearly zero, because they correspond to parameter combinations that do not exist in the data set. However, (1) a trained BN cannot perfectly represent the data and (2) training will attempt to fit spurious relationships that offer no real predictive skill. This second problem is called overfitting. Thus, we seek measures of skill that can quantify how well the BN predictions fit the data and then determine how much of this fit is spurious such that interpretations of the model output can be used to understand robust and generalizable coastal process relationships.

To evaluate our BN skill, we conducted a series of *k*-fold cross-validation tests using the approach of *Fienen and Plant* [2015]. The skill metric used was the error rate, which measures the percent of cases where the most likely predicted outcome (i.e., the bin with the greatest posterior probability) does not match the observed outcome. To implement these tests, we use a random sampling scheme to divide the data set into k subsets (folds) where $k-1$ of these subsets are used to train the BN and the remaining data are used for testing the BN to identify differences in the hindcast and validation skills. The process is repeated until all permutations of the training and testing subsets have been used and results are averaged across these folds. Predictions of all three output variables (DH, BW, and BH) can be performed simultaneously, or each output can be predicted separately, allowing the remaining output variables to be used as input. We applied the cross-validation analysis to seven different BNs to assess the relationship between calibration and validation errors as a function of model complexity, testing each output separately. The eight BNs included the primary BN that was designed subjectively (Table 1). The remaining BNs explored model complexity by varying the number of bins from two (low complexity) for each input node to eight (high complexity). The bins are defined to include equal probability prior distributions, which differs from the design of our primary BN based on threshold values and data uncertainty.

Additionally, we explored the sensitivity of BN skill to the amount temporal variability contained by the data used in training. One of our assumptions was that the spatial variability in a particular study site can be used to represent temporal variability if there is enough geomorphic diversity to capture different processes at different locations. For example, the north and south ends of the island are narrow and low and tend to overwash frequently, whereas the middle section of the island has high dunes that may not overwash often. Using data from time periods that represent both recent and past overwash, we can test whether we have enough data to develop a robust BN that represents temporal and spatial variability. The error rate metric was used to evaluate seven different BNs, all with model complexity identical to the primary BN, but using all possible

combinations of data sets such that the BN was trained on a single data set (e.g., 1999, 2002, or 2008), sets of two data sets (1999 and 2002, 1999 and 2008, or 2002 and 2008), and all three data sets simultaneously.

3.4. Morphologic Analysis With the BN

Once a BN is trained and tested such that an optimal fit to data has been achieved that balances robustness and generalizability on one hand and representation of geomorphological process details on the other, it can be used to analyze the important correlations between input data and output data as well as to identify the role of correlations among the input and output variables. At worst, if there are no meaningful correlations between input and output variables, the BN will return the prior distribution as the prediction in each case, and this result would represent the maximum prediction uncertainty (equation (3)). (An exception to this statement is the case where a prediction is requested for a scenario that was not included in the training data. In this case, the priors would consist of uniform distributions which represent a state of total uncertainty). At best, strong correlations between input and output variables will, via Bayes' rule, narrow the predicted distributions and identify a single bin with 100% probability.

Lastly, we used a log likelihood ratio metric [*Weigend and Bahnsali*, 1994; *Plant and Holland*, 2011] to examine the impact of individual input variables on model performance. The log likelihood ratio measures the performance of the BN predictions relative to the prior probability and is calculated as

$$\mathrm{LR} = \sum_i \log\left\{p_i^{\mathrm{posterior}}(O_i)\right\} - \sum_i \log\left\{p_i^{\mathrm{prior}}(O_i)\right\} \tag{4}$$

where $p_i^{\mathrm{posterior}}$ is the predicted (i.e., posterior) probability distribution function (PDF) computed using the input variables (e.g., DI, SLC, ME, WB, and AM) on the ith transect evaluated at the bin corresponding to the observed values (e.g., O_i = DH, BH, or BW) on that transect. The log of the prior probability $\left(p_i^{\mathrm{prior}}(O_i)\right)$ for the specific outcome is subtracted from the log of the predicted probability and summed over all transects. A positive log likelihood results if predicted probability is greater than that of the prior; i.e., the prediction is more likely than the prior. A log likelihood ratio less than zero results if the predicted probability is smaller than the prior probability. Negative log likelihood ratios can result when the most likely outcome has a high probability but differs from the actual outcome (i.e., the prediction is confident and wrong) or when the predicted PDF has a low probability everywhere (hedging).

4. Results

Our results begin with a presentation of the BN model skill obtained from the cross-validation analysis. This includes analysis of the hindcast (e.g., training or calibration) and validation skill of our primary BN as well as comparisons to alternative BNs with varying levels of model complexity and varying number of sample dates included in the training data. Then we evaluate model sensitivity to understand the geomorphic relationships captured by the BN, beginning with some simple, illustrative scenarios and then including complicated and quantitative evaluations.

4.1. Skill Assessment

4.1.1. Calibration/Validation Test Using *k*-Fold Approach

We show the calibration and validation skill using the *k*-fold testing approach applied to predictions of DH given all other variables as input (Figure 4a). The primary BN (see Figure 7 for a graphical description of this BN) was used, and several choices of number of folds were explored, starting at two folds and increasing to 15 folds. For two folds, the data are divided in half; the BN is trained and tested on one half (calibration) and then tested on the withheld half (validation). For 10 folds, 90% of the data are used in training and 10% are used for testing, again using all permutations for the training and testing sets. In all cases, the mean (averaged across the folds) calibration error rate is lower than the validation error rate. The difference in error rate indicates overfitting. That is, the difference in error rate is due to details that are fit by the BN in one data set but are not generally applicable to the withheld data set. As the number of folds increases, more data are used for training and the calibration error rate increases because the BN cannot explain the increasing amount of observed detail. The validation error increases slowly as well, and the validation error is more variable across the folds than the calibration error. Both error rates begin to converge to constant (but different) values when the number of folds is greater than five, approaching a 50% overfitting ratio (calibration error

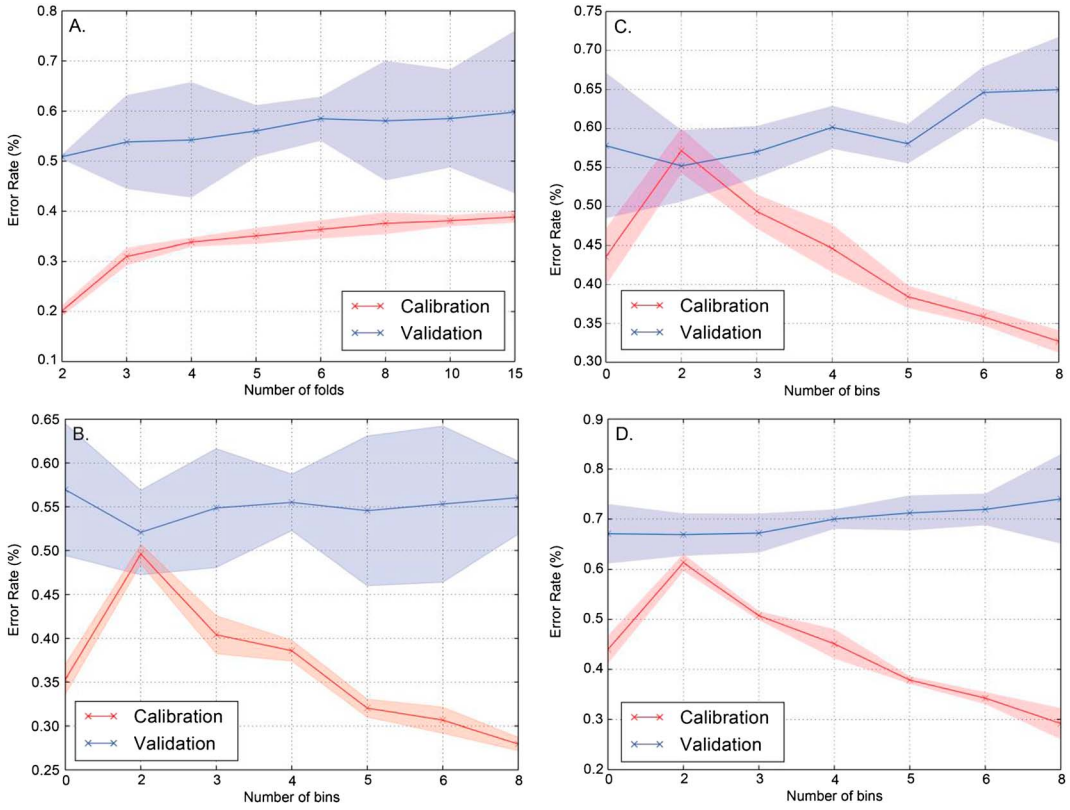

Figure 4. Dune height prediction error rate as a function of (a) calibration/validation folds and (b) number of bins (using five folds). The solid lines show the mean across all folds (i.e., all combinations of training and withheld data for each choice of fold number). The shaded areas show maximum and minimum values of the error rates across all folds. The case where the number of bins is 0 indicates the primary BN (Figures 4b–4d). The analysis for dune height (Figure 4b) was repeated for (c) beach width and (d) beach height.

rate/validation error rate = 0.2/0.4). We will assume that this ratio applies to the limit of $k = N - 1$ (where N is the number of data points and one value is left out for validation) and this is the overfitting of the most robust model, trained using all of the data.

We then applied the cross-validation analysis to eight different BN designs to assess the relationship between calibration and validation errors as a function of model complexity (Figure 4b). Because the difference calibration and validation error rates change only slightly when we use more than five folds and because we are only concerned with the relative performance of competing BN designs, rather than assessing the absolute skill of the primary BN, we use five folds in subsequent tests. The calibration error rate is 0.35 for dune height when the primary BN is evaluated (indicated as 0 bins in Figure 4b). The corresponding validation error is about 0.58, indicating that the calibrated model is overfit, as shown in Figure 4a. When only two input bins are allowed, the calibration and validation error rates are nearly equal (about 0.50 and 0.52). Thus, this relatively simple BN is robust compared to validation but does not explain as much of the data variability as the primary BN. By increasing the number of bins to four, the calibration error rate is about the same as the primary BN's error rate and the validation error rate is basically unchanged. For a larger number of bins, the calibration error rate decreases (more of the details of the training data are explained), but the validation error rate remains relatively unchanged. The consistent decrease in the calibration error rate reflects an increasingly overfit model, but there is no cost in terms of robustness or generalizability of overfitting as far as the validation skill is concerned. Note that we do not change the number of output bins so that the calibration and validation tests have fixed bin resolutions for the variable being predicted (dune height). Additionally, the AM node, which is an input variable, has the same number of bins for all tests because the values are discrete and cannot change. We repeated this test for beach width and beach height variables (using just three folds). Beach width and beach height error rates (Figures 4c and 4d) were approximately 10–15%

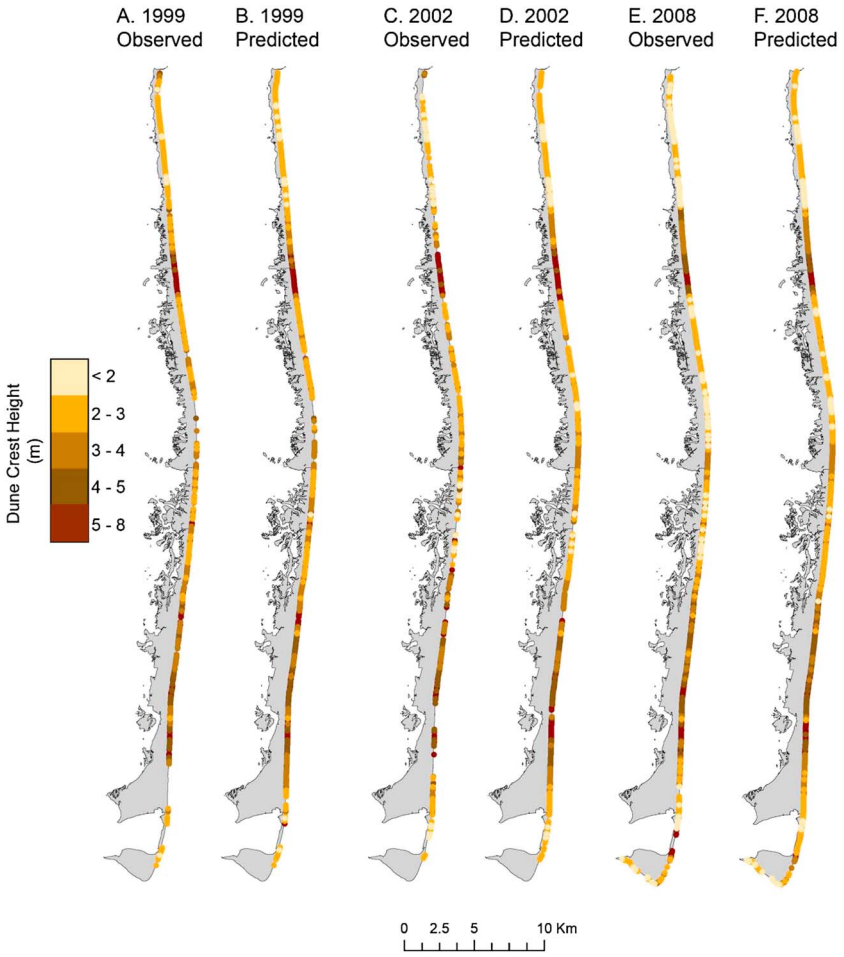

Figure 5. Maps of Assateague Island showing comparisons of observed and predicted dune crest heights for each data set included in this study. Each map displays the most likely dune height determined from the output probability distribution for DH. Observations were binned and displayed according to the discretization defined in the BN.

higher respectively than those for dune height, and validation skill worsened for complex BN designs with greater than six bins. The skill values for the primary BN are consistent with complexity of four to five bins per input and maximize calibration skill without degrading validation skill.

4.1.2. Skill Sensitivity to Addition of Temporal Variability

The detailed data available to train the primary BN spanned three different dates over nearly a decade when the island geomorphology evolved, either naturally or due to anthropogenic activity (Figure 3). As with the *k*-fold method, which randomly subsampled the data, we can train and test the BN using different data sets through time. For example, the BN trained on all of the data (e.g., all three dates and all locations) is used to predict DH at each of the three dates by varying the input variables (Figure 5). This spatially explicit prediction is generated at each transect and for each year by extracting the values of the input variables from the data, inserting them into the BN, and extracting the updated probabilities for DH and displaying the result at the location of the shoreline. At a broad scale, predicted patterns of DH (showing the most likely outcome for the prediction) are similar to the observed patterns. A trend of dune lowering in the northern part of the island is predicted well, and a general lack of dune height change is predicted (and observed) in much for the southern part of the island.

To assess the impact of training the BN on different barrier island conditions, error rates were computed for hindcast predictions of DH, BW, and BH based on training scenarios that used data from only 1 year (three different tests), 2 years (three different tests), and all years (one test) (see section 3.2 for data set description). In addition, there are two levels of input specification. All possible inputs can be used in a

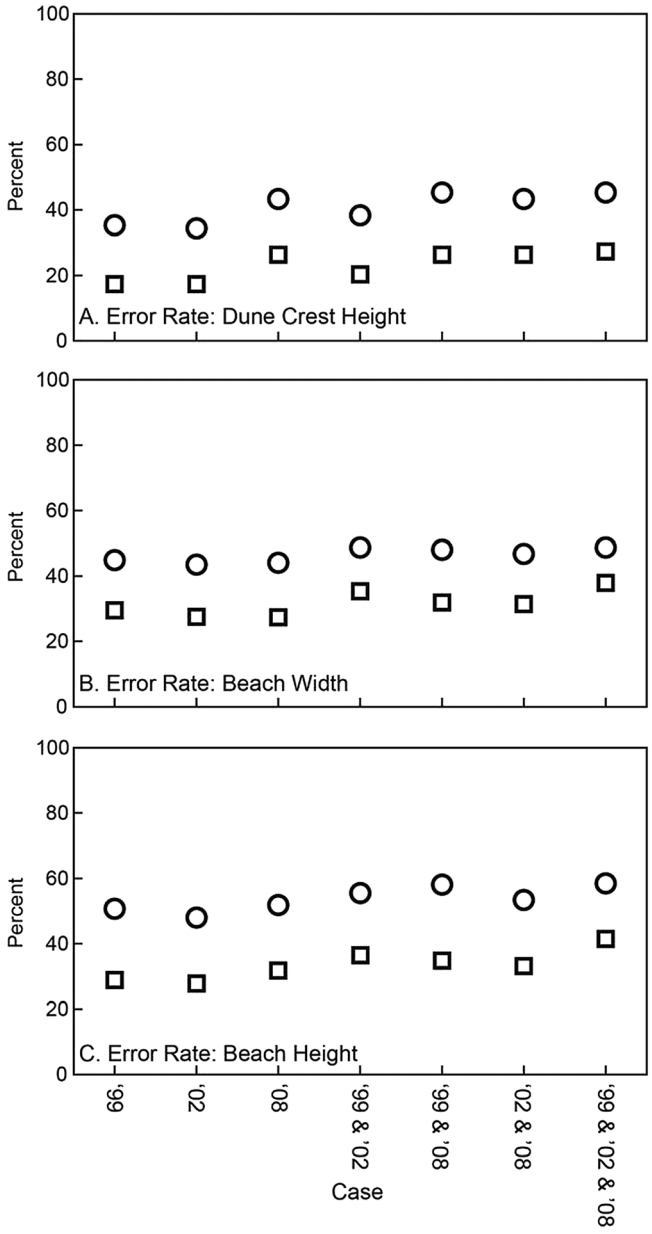

Figure 6. Hindcast error rates for BN trained on data from one or more dates (horizontal axis labels) and calculated where only one variable was predicted (squares) or where three variables were predicted simultaneously (circles).

prediction (Figure 6, squares), such that the detailed morphologic information of all but the variable being predicted (DH, BW, or BH) is used as input. Alternatively, we can omit the detailed morphologic information from the inputs and instead simultaneously predict DH, BW, and BH (Figure 6, circles). Error rates tend to be highest for predictions trained on data from all 3 years (Figure 6, last case in each panel) and lowest for predictions trained on a single-year data set. This is consistent with the result from the *k*-fold testing that showed increasing calibration (hindcast) error rates as more data were used in the training (Figure 4a). Error rates are lowest for DH and range from 17–27% for single-variable prediction to 34–45% for three-variable prediction. (These error rates are slightly lower than what was shown in Figure 4a because we limited the number of iterations when conducting the *k*-fold analysis due to the large number of simulations required. Using the more intensive training, we found that the *k*-fold analysis error rates could be reduced by 20% for the calibration and 10% for the validation—the sensitivity trends were not changed.) For BW, error rates range from 27–35% for single-variable prediction to 44–49% for three-variable prediction. Error rates for BH range from 27–38% for single-variable prediction to 48–59% for three-variable prediction.

4.2. Morphologic Analysis

The trained BN can be used to make predictions using all the inputs, some of the inputs, or based on the prior probability without providing any input constraints. In our application, the prior probability of a particular variable represents its probability distribution given all possible conditions in our data set. The prior distributions (Figure 7a) indicate that 65% of the island has undergone long-term shoreline retreat (a sum of the probabilities in bins corresponding to negative SLC) and about 30% has been subject to anthropogenic modification (where AM is not "none") over the last 40 years (a sum of the probability in all bins, excluding none). A broad range of island widths are encountered with equal probability in the bins that we have assigned; and 60% of cross-island transects have a mean elevation less than 1.0 m. The most likely dune height is 2–3 m (30% probability); beach width is most likely 50–75 m (32% probability); and beach height is most likely 3–3.5 m (28% probability). The BN allows us to ask how these most likely characteristics vary if we impose constraints on specific barrier island conditions, which we explore in the next sections.

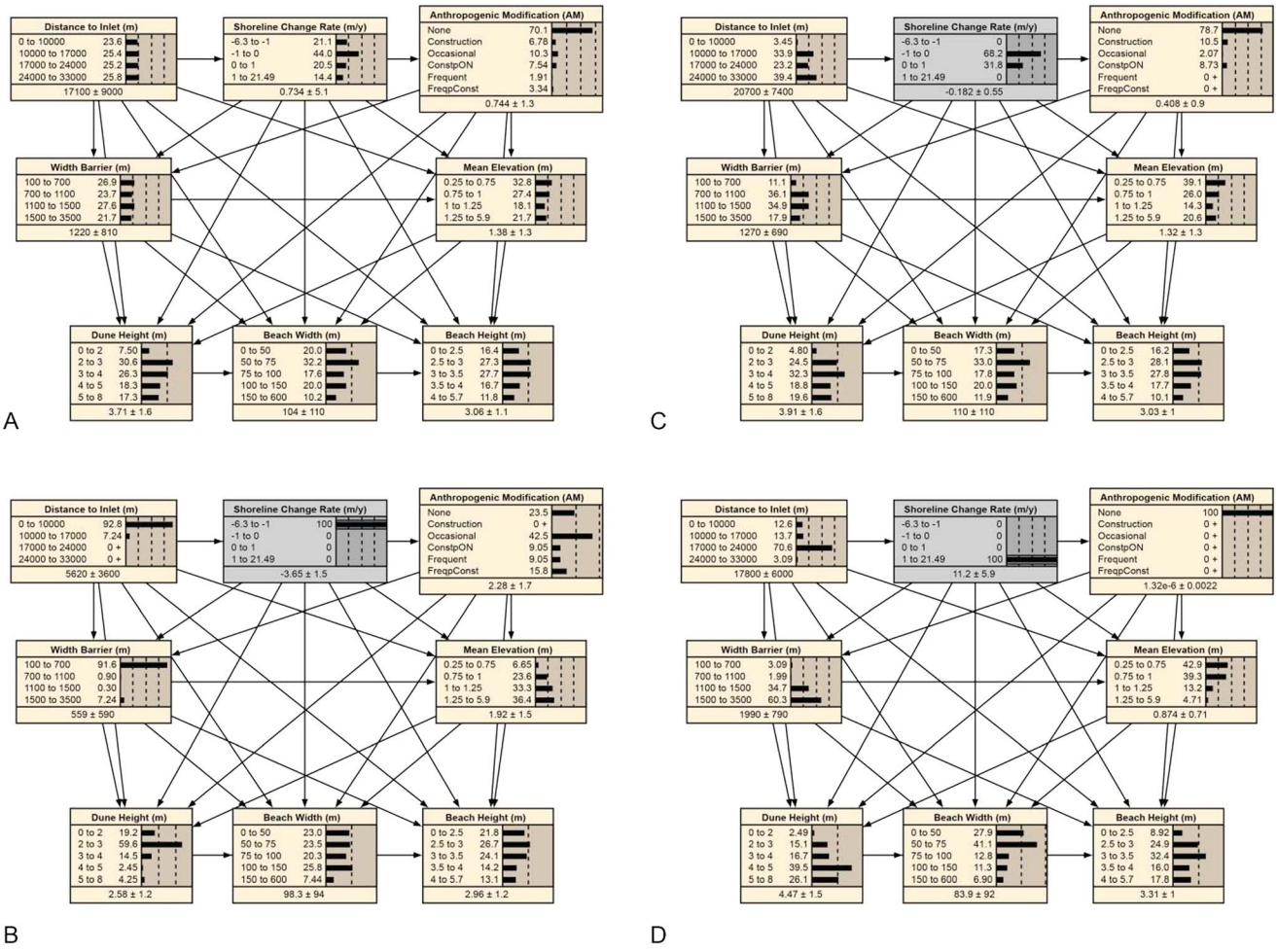

Figure 7. Examples of the BN showing each variable, the probabilities in each bin, and correlations included in the CPT (arrows). The mean and standard deviation value is shown for each variable (it is meaningless for the discrete AM variable). (a) The prior probabilities. The BN is updated to show probabilities for different rates of shoreline change, including (b) an erosional scenario where $P(\mathrm{SLC} < -1) = 100\%$, (c) a stable scenario where $P(-1 < \mathrm{SLC} < 1) = 1$, and (d) an accretional scenario where $P(\mathrm{SLC} > 1) = 1$.

4.2.1. Geomorphic Sensitivity to Variations in Shoreline Change Rate

Posterior PDFs are updated by adding constraints corresponding to known input values at particular locations or by exploring scenarios that survey the range of input variability. We take the latter approach here. For our first scenario we specify that $P(\mathrm{SLC} < -1\ \mathrm{m/yr}) = 100\%$, which corresponds to long-term shoreline recession. Here the PDF for SLC is set to 100% in the −6 to −1 m/yr bin and the BN reevaluates and updates the PDFs for the remaining variables (Figure 7b). The resulting PDFs indicate that rapid shoreline recession is most likely within 10 km of an inlet [$P(\mathrm{DI} < 10\ \mathrm{km}) = 93\%$] and the likelihood of some anthropogenic response is 76%. The PDFs also indicate that island widths are likely to be narrow, and mean island elevations are higher than the prior and most likely >1 m. Dune crest heights are most likely to be less than 3 m high (79%); beach width and beach height are generally similar to the prior probabilities.

Next, we explore a scenario where long-term shoreline changes are stable (SLC = ±1 m/yr), and we exploit the ability of a BN to use uncertain input by assigning equal likelihood for SLC = −1 to 0 m/yr and 0 to +1 m/yr. Because our input is uncertain, the BN algorithm updates this input information with the prior to yield a prediction of the SLC PDF (Figure 7c) that indicates it is more likely to be eroding (68%) than accreting (32%). In our study area, stable shorelines occur everywhere except within 10 km of tidal inlets and are only 21% likely to be associated with an anthropogenic response. Compared to the eroding scenarios (Figure 7b), island widths are wider, the mean elevation is lower, and dune heights are higher (most likely to be 3–4 m high). Beach widths are likely to be slightly greater, and beach heights are slightly higher.

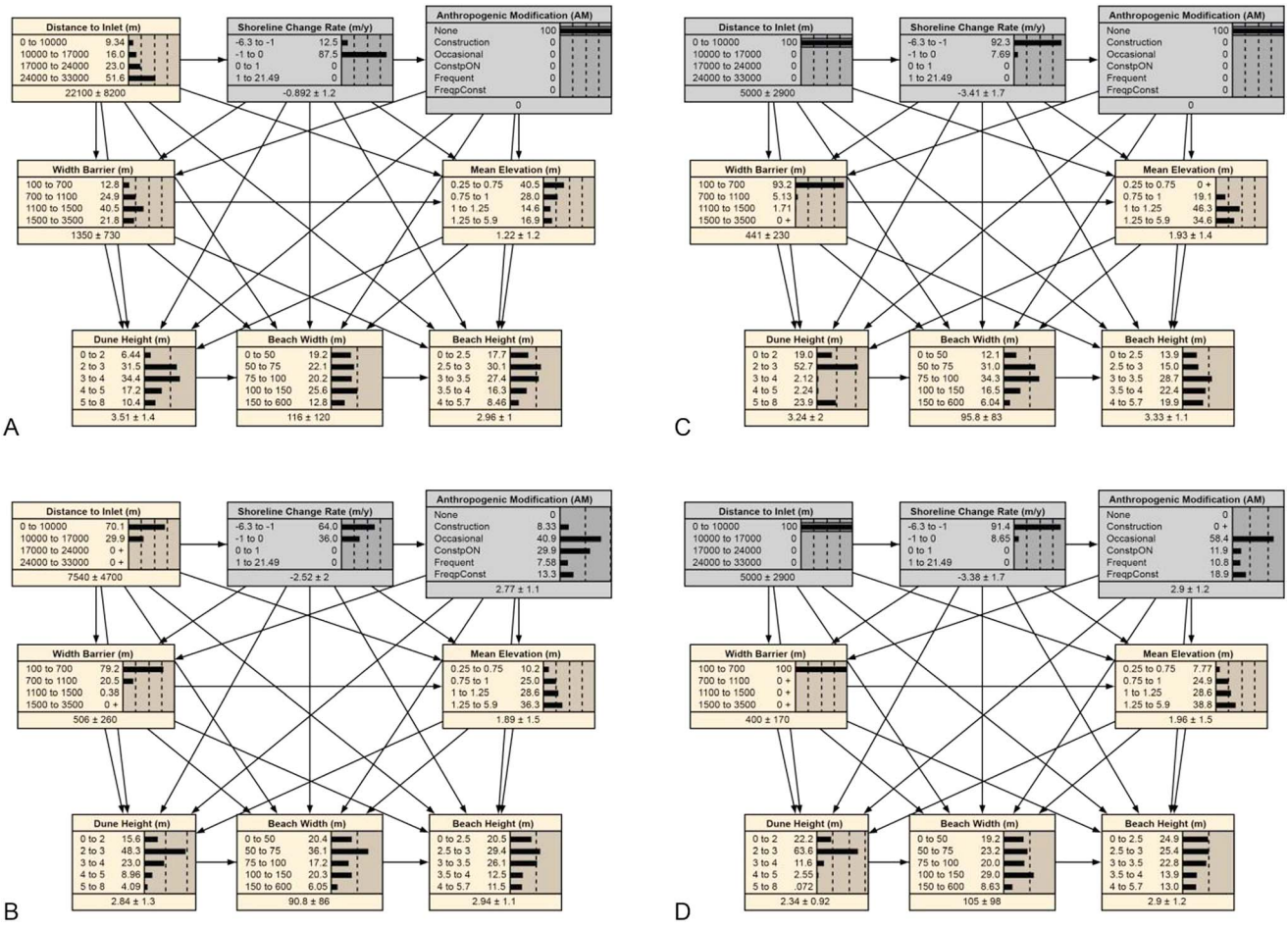

Figure 8. BN examples where SLC, AM, and DI are included as constraints. All cases consider erosional scenarios (SLC < -1) and include (a) no AM, (b) any form of AM, (c) no AM and close to an inlet, and (d) AM and close to an inlet.

Finally, accreting shorelines (SLC > 1 m/yr, Figure 7d) occur mostly at intermediate distances from an inlet (a few are very close to an inlet—likely corresponding to prograding spits) and are not associated with anthropogenic modifications. Island widths are most likely to be wide, and the mean elevation is more likely to be lower than the other scenarios. Dune heights are likely to be the highest of any scenario. In addition, beaches are most likely to be narrower and slightly higher compared to all the other scenarios.

4.2.2. Geomorphic Sensitivity to Anthropogenic Modification

Anthropogenic modification is, unsurprisingly, correlated with the erosional cases where SLC < -1 m/yr (Figure 7b above). This leads to the following question: are there clear differences between eroding portions of the coast that include some form of AM versus those where AM is absent? We constrain the following analysis to erosional scenarios and investigate the role that the remaining variables (AM, DI, and WB) have in influencing the detailed barrier island characteristics (DH, BW, and BH). Comparing input scenarios where AM = none to scenarios where AM = "not none" constraints, we find that AM is most likely near inlets and where the barrier island is narrow (Figures 8a and 8b). To produce this prediction, we again exploited the ability of the BN to utilize uncertain input and set the probability of AM = none to be zero; the BN uses the prior probabilities and the CPTs to update the probabilities of the other states. Low dunes (DH < 3 m) are more likely where AM is present (64%) compared to no AM (38%). Beaches are more likely to be narrower (BW < 75 m) if AM is present (57%, compared to 41% without AM). Beach height is similar for the two cases. We examine a more direct comparison between erosional cases with and without AM by considering cases where DI is less than 10 km (Figures 8c and 8d). Comparing scenarios with and without AM under this constraint, a bimodal distribution of dune heights is predicted without AM, where dunes are either <3 m (72%) or very high (24%). When AM is present, dune heights are more likely to be <3 m (86%). Beach width

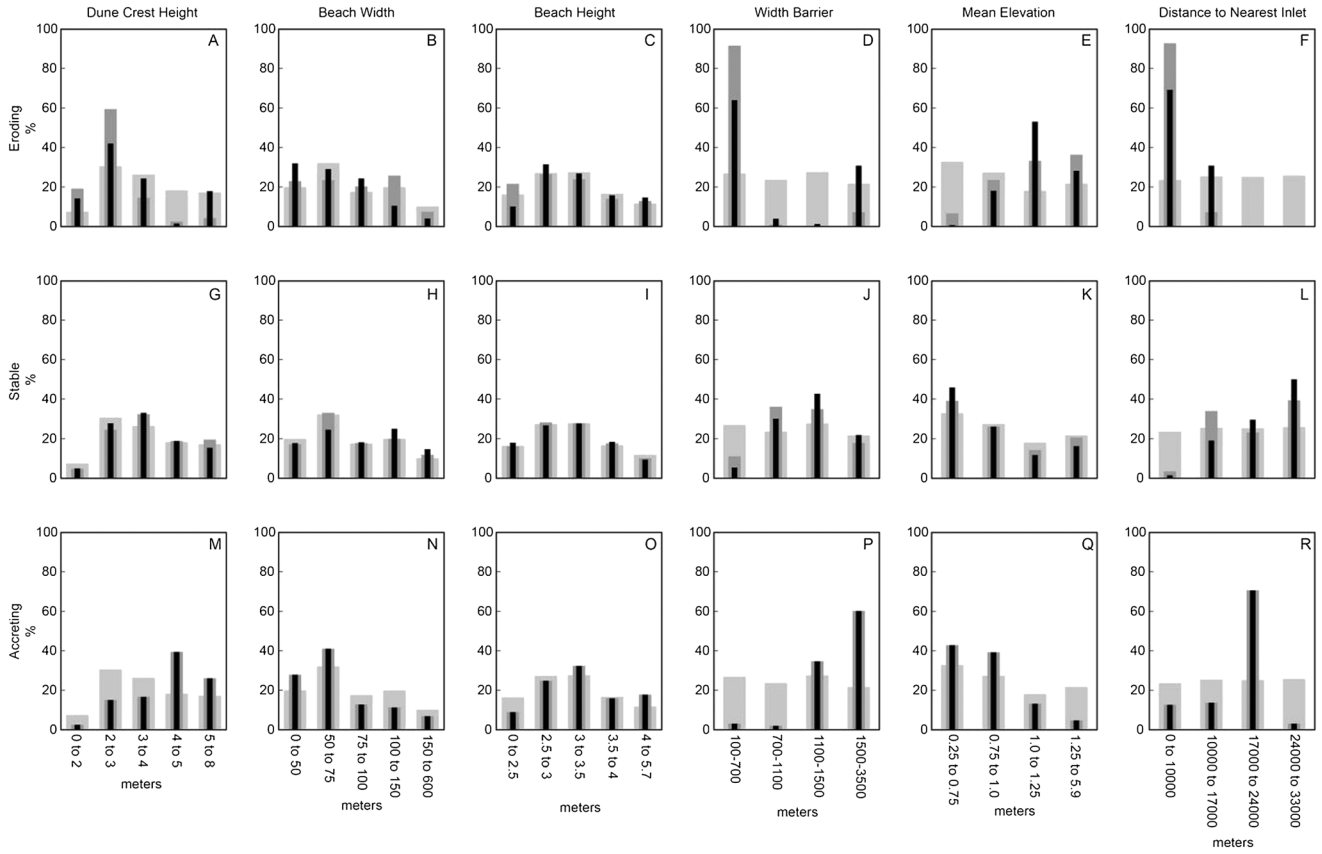

Figure 9. Summary plots of the probabilities for each variable constrained by shoreline change scenario to represent (a–f) eroding, (g–l) stable, and (m–r) accreting scenarios. The shading indicates prior probabilities (light gray), each SLC constraint (medium gray bars), and AM constraint corresponding to no anthropogenic modification (black bars).

distributions indicate that wider beaches are more likely with AM and beach height is more likely to be higher without AM.

The results that include rapidly eroding (SLC < -1 m/yr), stable ($-1 <$ SLC < 1 m/yr), and accreting (SLC > 1 m/yr) scenarios where AM is either unconstrained or constrained to be none are summarized and compared to the prior distributions for each variable (Figure 9). Where shoreline change rates are constrained to erosion (rate < -1 m/yr, net shoreline movement shoreward), resulting posterior PDFs are distinct from the prior. For cases where shoreline change rates are stable ($-1 <$ SLC < 1 m/yr; shoreline stationary), posterior PDFs remain relatively close to the prior distributions for cases with and without human modifications (Figures 9g–9l). The largest differences between the posterior and prior PDFs occur for island width and distance to nearest inlet. When cases with and without AM are compared, posterior PDFs are within 10% of one another. Where shoreline change rates are constrained to accretion (SLC > 1 m/yr; net shoreline movement seaward), PDFs for dune height, barrier width, and distance to inlet show the most response compared to the prior. In addition, there is no difference in the posterior PDFs with and without AM. This result is consistent with the observation that AM was already unlikely for this set of scenarios. Overall, some variables are not very sensitive to SLC and AM constraints (e.g., BH and to some degree BW) while others exhibit greater sensitivity (DH, WB, and DI, where "sensitive" was defined as predicted PDFs exceeding 60%). Below, we explore the role of the other variables in predicting DH, BW, and BH.

4.2.3. Geomorphic Sensitivity to Input Variables

The previous section illustrates that there are multiple correlations between variables at all scales. When the correlation exists between input variables, either the inputs are somewhat redundant (e.g., SLC and DI may be redundant and one of the variables could be eliminated to make a simpler model) or the input correlation can be used to correct uncertainty in the inputs (e.g., where we specifically used an uncertain constraint,

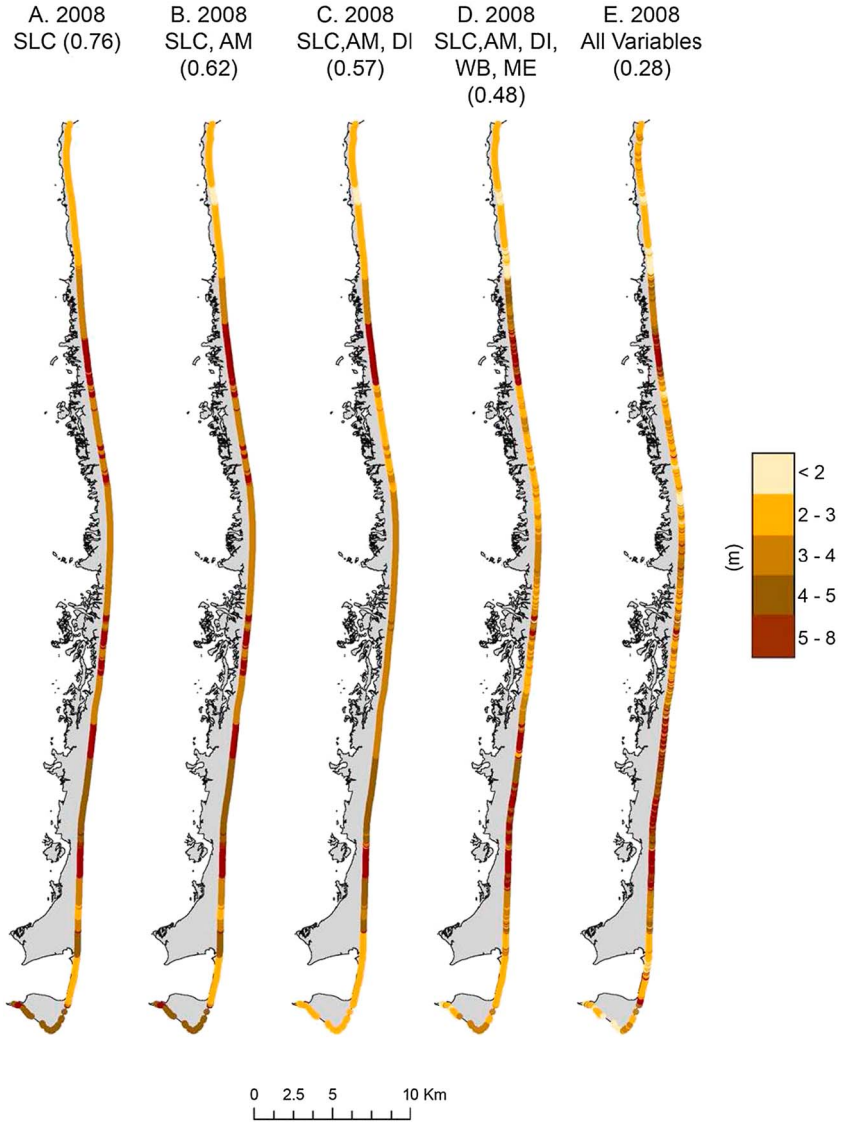

Figure 10. Maps of Assateague Island showing BN-predicted dune crest heights using (a–d) partially constrained or (e) all input data from 2008. Error rates for each set of predictions are indicated in parentheses.

Figure 8b). We already used all of the information from the input variables SLC, DI, WB, AM, and ME to make spatially explicit predictions of DH (e.g., Figure 5) as well as for BW and BH when we assessed the BN skill (Figures 4c, 4d, and 6). The impact of progressively including more of the input variables on the DH prediction was evaluated for five prediction scenarios, ranging from using only a single input variable (SLC) to using all possible variables in the data set (Figure 10). Much of the broad structure of dune height variability is explained with SLC as the only input. Increasing the number of inputs yields more fine-scale variability. The prediction accuracy increases with increasing the number of input variables. Error rates do not drop below 50% until at least five variables are input in the BN (Figure 10d). In addition, the largest decrease in the error rate (to 20%) occurs when detailed morphologic variables (BW and BH) are included as inputs.

Value of the error rate metric employed so far is to evaluate the prediction skill of the most likely value predicted by the BN. However, many problems do not require a specific estimate but instead ask how likely is DH (or BW or BH) to exceed a threshold value. We have used this line of questioning in our demonstration of the differences and similarities of the various prediction scenarios (e.g., Figures 7–9). A specific example related to storm vulnerability queries the likelihood of overwash exceeding BH or DH. For a particular storm,

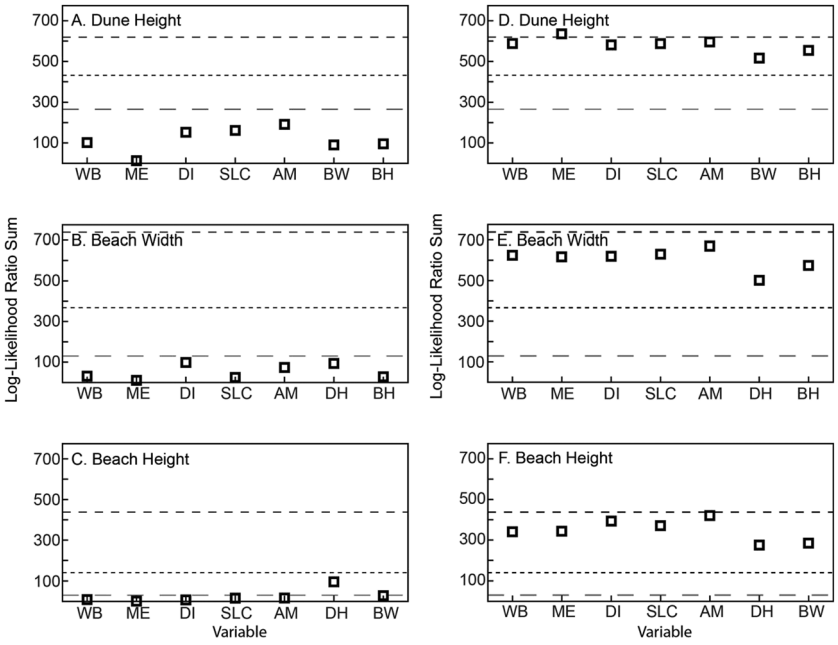

Figure 11. Log likelihood ratio results for (a–c) single input variable and (d–f) withheld input variable predictions. The upper dashed line shows log likelihood ratios corresponding to predictions using all input variables and predicting one output variable. The middle dashed line shows the log likelihood ratios for simultaneous prediction of DH, BW, and BH using all other input variables. The lower dashed line shows log likelihood ratios using only SLC and AM input.

the runup height can be computed [*Stockdon et al.*, 2007] and can be used to set a threshold value for BH and DH. The runup calculation also requires an estimate of beach slope, so BW (along with BH, from which slope can be estimated) is also relevant.

The value of using a BN to evaluate threshold-crossing probabilities is that it is possible to consider multiple outcomes simultaneously. For example, in Figure 8c, there is a bimodal distribution for DH for the case of rapid long-term erosion without any AM. DH might be very low (the most probable outcome corresponding to low, frequently overwashed sections of the island), but there are high dunes that are being actively eroded as well. We evaluated log likelihood ratio scores in three ways to examine how each of the input variables contributed to uncertainty reduction. First, we evaluated the log likelihood ratio for predictions using all input variables. This should represent the best possible prediction. Then, we evaluated log likelihood ratio scores for predictions that included only a single input variable (Figures 11a–11c). Finally, we evaluated the log likelihood ratio for predictions where all but one input was included in the prediction (Figures 11d–11f). The log likelihood ratio results (only one input and all but one input) can be compared to the result when all of the inputs are used in the prediction. For dune height, the single-variable predictions using only AM, DI, or SLC produced the highest log likelihood ratio scores (Figure 11a). For BW predictions, DH, DI, or AM had the highest scores, while SLC was not among the most important inputs (Figure 11b). For BH, DH was the most important input; all other scores were relatively low in comparison (Figure 11c).

This analysis was repeated using all but one of the input variables. In this case, variables that most reduce the log likelihood ratio can be interpreted as having the largest impact on the prediction. For example, removing BW reduces the log likelihood ratio for dune height predictions the most, followed by BH (Figure 11d). Alternatively, when ME was removed, log likelihood ratio scores exceeded the score corresponding to input of all variables (Figure 11d, uppermost dashed line), indicating that ME actually degraded the prediction. Log likelihood ratio scores for beach width predictions also depend on the detailed beach variables, with removal of DH and BH causing the largest decreases in log likelihood ratio score (Figure 11e). Removing any of the remaining variables produced smaller log likelihood ratio decreases and AM produced the smallest decrease. Beach height predictions responded essentially identically to the beach width prediction (Figure 11f).

5. Discussion

Our results demonstrate that the primary BN can predict the probability of specific geomorphic characteristics, including dune crest height, beach height, and beach width metrics that are relevant to coastal vulnerability. Predictions used information that describes larger-scale characteristics such as distance to inlet, barrier width, and mean elevation or that characterizes some of the long-term drivers of morphologic change such as long-term shoreline change rates and knowledge of anthropogenic modifications. We have used the BN to couple these variables that span different temporal and spatial scales, as well as to couple quantitative measurements (heights, widths, and rates) with qualitative classification data representing anthropogenic modifications. Because the BN is a statistical model, we must interpret the results to identify the geomorphic processes that we believe are responsible for robust relationships. We must also explain how these results might depend on details of our modeling approach by interpreting the skill assessments. Finally, the value of our analysis approach lies in its ability to be extrapolated to new problems and tests in the future. We discuss each of these topics in the next sections.

5.1. Interpretations of Predictive Relationships

The BN used in this study shows that specific shoreline change trends are correlated to barrier island geomorphology. For example, sections of the barrier island that are eroding rapidly (at rates < -1 m/yr) are most likely to be narrow, close to tidal inlets, and have low dunes (Figure 9). Those sections of barrier island that are accreting at rates >1 m/yr are generally farther from inlets, are wider and have higher dunes, but exhibit lower mean elevations. On the other hand, sections of the barrier island where shorelines are stable exhibit a range of geomorphic possibilities that differ little from the prior probabilities. Furthermore, where barrier islands have not undergone anthropogenic modifications, they tend to have higher probabilities of having wider island widths, higher dunes, and narrower beach widths (Figure 8). Although SLC and AM are the strongest individual influences on the short-scale geomorphic characteristics (e.g., DH), including the other variables results in more accurate predictions (Figures 10 and 11). For example, the sensitivity analysis shows that removing inputs BW and BH results in the largest departure from the best prediction (Figures 10 and 11).

Our results suggest that portions of the barrier island experiencing erosion (i.e., negative SLC rates) are more vulnerable to storm overwash in the short-term because dune heights are more likely to be lower (2–3 m) compared to the prior distribution. This result makes an important connection between the long-term processes of shoreline change and the short-term processes that, when integrated, produce the long-term impacts. Additionally, it exposes feedbacks in the system where low dunes allow overwash that contributes to island rollover and landward migration of the shoreline; this tends to maintain low dunes because of the rapid landward migration associated with high overwash flux [*Lorenzo-Trueba and Ashton*, 2014].

The dependence of geomorphology on location along the length of the island is shown to be important. For example, our analysis indicates that extreme erosion occurs within 10 km of tidal inlets (Figure 7b). It is well recognized that shoreline change trends can be variable near tidal inlets [*Nordstrom*, 1988] where there can be large sediment transport gradients associated with changes in shoreline orientation, tidal flow through inlets, and interactions with incoming waves. *Fenster and Dolan* [1996] investigated the extent of inlet influence on barrier island shoreline behavior and showed that tidal inlets influence shoreline change behavior over distances of 5–13 km in this region. We show that it is possible to include this information in what is otherwise a transect-based modeling approach. This capability in our application to Assateague Island does not prove that the specific relationship between DI and the other variables is universal. However, for the geomorphic features included in this study, it is clear that DI is important. The actual role played by DI likely depends on a variety of factors, including rates of alongshore migration of the island, rates of inlet migration and spit extension, and island orientation.

5.2. Interpretation of Prediction Scenarios at Different Spatial Scales

Our skill analysis shows that the BN can reproduce observed DH, BW, and BH values accurately 62–73% of the time (1 minus the error rate) for cases where just one variable is evaluated and all other variables are used as input. This prediction scenario is relevant when some of the detailed morphologic information is known. For example, if a coastal engineering project is planned to construct dunes and beaches to specific elevations, the model could be used to predict a compatible range of beach widths. If, on the other hand, only large- and intermediate-scale information is available, then all three detailed variables (DH, BW, and BH) must be evaluated simultaneously, which reduces error rates to 45–60% (Figures 6, 10, and 11). This shows that the

inclusion of at least some of the detailed variables reduces the prediction error for DH, BW, or BH due to the correlations at the detailed morphological scale. Similar improvements are found for predictions of BW (including DH and BH as input) and BH (including DH and BW as input) (Figure 6). Coupling across a variety of spatial scales allows the BN to answer a range of questions. In the case of beach nourishment, which often creates a beach with a specific elevation and width, one could ask what dune height would be consistent with the new beach configuration that also accounts for long-term erosion. We illustrate scenario-based forecasting in section 5.4.

5.3. Skill, Fitting, Overfitting, and Data Requirements

Overfitting is a concern of any statistical estimation approach, regardless of whether it is simple linear regression with a few free parameters or a BN with thousands of free parameters. Overfitting is a problem (1) if hindcast skill is used to naively represent the more generalizable validation skill and (2) if the hindcast skill is excessively spurious such that the more generalizable validation skill is not minimized. To address the first problem, we identified the degree of overfitting (it is about 50% of the error rate) and demonstrated that overfitting is minimized by using all of the available data to train the primary BN (Figures 4a and 6). To address the second problem, we show in Figures 4b–4d that the primary BN has a level of complexity that achieves a high descriptive power (hindcast error rate is low) without degrading generalizability (validation error rate is minimized). We find that a BN discretized with four to five bins per input variable minimized both training and validation errors. The validation errors were not very sensitive to increasing the number of bins until more than three bins for DH and BH and four bins for BW were used (Figures 4b–4d). Again, the training error rate reduced steadily as model complexity increased.

Our primary BN used in the morphologic analysis was trained on three data sets to provide input data representing a range of geomorphic conditions and temporal variability. Using all of the data for training (Figure 4a) or all three data sets resulted in degraded hindcast skill (Figure 6) because the BN structure and training could not represent all of the details represented in all of the data sets. Even so, the difference in error rates between the highest and lowest performing BN training scenarios was only 5–10% (Figure 6). The largest of these differences occurred for DH and BH when three variables (DH, BH, and BW) were predicted simultaneously. The training data used in this study span nearly a decade and reflect a barrier island that had been eroded and breached by strong winter storms and was consequently subject to erosion and breach management activity (data sets from 1999 and 2002). Thereafter, the barrier island had been relatively unaffected by storms for several years (data set from 2008) and was subject to persistent anthropogenic modification (principally sand management programs). By adding more data spanning periods of significant morphologic change (natural or otherwise), the model is forced to ignore some patterns, treating them as a contribution to uncertainty, while fitting variability that can be reproduced more robustly. We purposely selected data sets where the morphology differed, and presumably, there is a point of diminishing return from adding additional data sets as no new observational complexity is introduced. For instance, error rates using 2 years of data are similar to error rates using 3 years of data. Admittedly, the variability through time is more challenging to predict than predicting spatial variability at a single time, but the temporal variability is captured statistically and is representative of future variability. The BN approach accounts for a range of variability by retaining the full probability distribution of predictions and therefore captures the increased, and realistic, uncertainties.

5.4. Forecast Scenario Examples

Dune height is a key indicator of overwash or inlet breaching vulnerability [*Sallenger*, 2000; *Stockdon et al*., 2007, 2009]. The capability to forecast future dune height probabilities driven by SLC or AM can be used to identify potential vulnerabilities. The predictive skill we have shown for the BN can be utilized to produce probabilistic forecasts of the future distribution of the detailed morphologic features (DH, BW, and BH) given some possible future scenarios for the larger-scale drivers (e.g., SLC and AM).

We calculated and mapped the probability of DH <3 m for three different scenarios representing plausible future conditions. The 3 m DH threshold is one that would be overtopped for a category 1 hurricane which, for Assateague Island, could drive 2.5 m of wave runup on top of 1 m of storm surge [*Doran et al*., 2012]. From a habitat management standpoint, regions of a barrier island subject to overwash are often attractive to shorebirds seeking foraging and breeding habitat [*Loegering and Fraser*, 1995; *Cohen et al*., 2009; *Gieder et al*., 2014] and thus our approach has decision support application where a coastal manager could answer

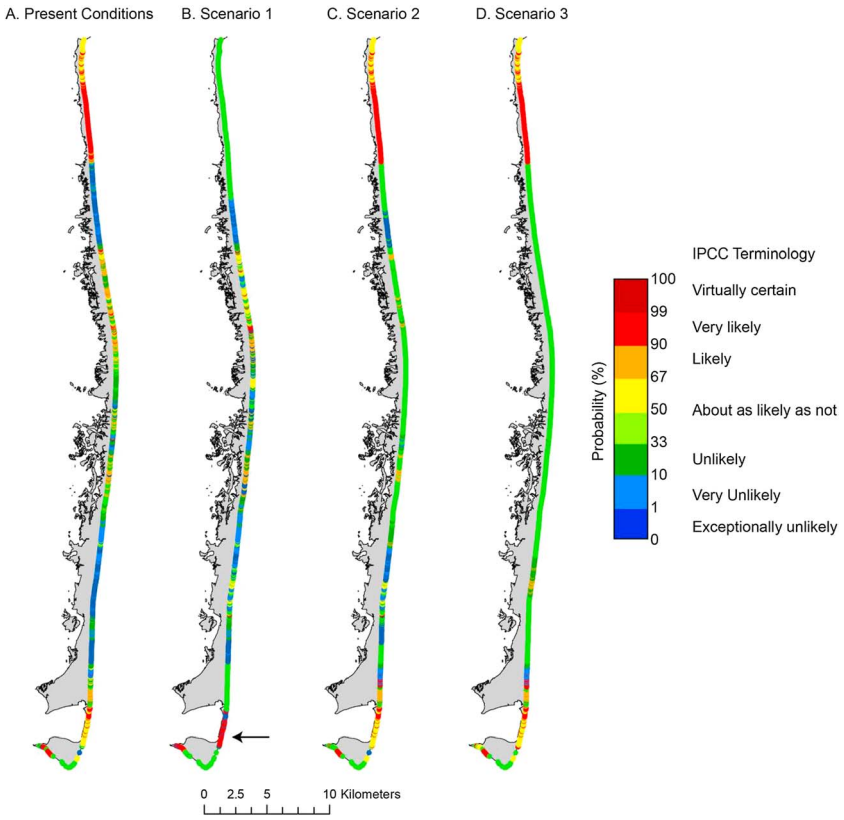

Figure 12. Maps of Assateague Island showing probability of DH ≤ 3 m evaluated using the BN for (a) present 2008 conditions, (b) SLC = 0, (c) SLC increases by 1 m/yr (small increase in erosion rate), and (d) SLC increases by 2.5 m/yr (large increase in erosion rate). For these scenarios DI, AM, WB, and ME were based on data from 2008. The color scale is labeled according to IPCC terminology [*Cubasch et al.*, 2013].

a question such as "What is the likelihood that future conditions would provide suitable habitat for shorebirds?" The three scenarios we examine are (1) stabilization of the barrier where SLC is 0; (2) small increase in long-term erosion rate, where SLC is more negative by 1 m/yr; (3) and large increase in long-term erosion rate, where SLC becomes more negative by 2.5 m/yr.

In these scenarios, BW and BH are unconstrained and they are predicted by the BN as well, but not shown here. All other variables are set to the current condition (i.e., the 2008 data set). Estimated probabilities of DH < 3 m for the three scenarios are shown on a map of Assateague Island (Figures 12b–12d) and compared to probabilities for present-day conditions (Figure 12a). For scenario 1 (Figure 12b), the probabilities of DH < 3 m are the most similar to those for present conditions along central portions of the barrier island and differ most notably at the northern and southern ends of the island where there are more extensive regions where low dunes become less likely. The one exception occurs along the southern portion of the island where there is an increased probability of DH < 3 m for this scenario (see arrow, Figure 12b). This occurs where the island is narrow, and distinguishing this location from the north end of the island, there is not any anthropogenic modification. Similarities for the central portions of the island are related to the fact that SLC = 0 m/yr is comparable to the historical shoreline change rates that are already consistent with the present-day case (Figure 12a).

Scenarios 2 and 3 add increasing amounts of erosion via negative SLC constraints. These scenarios result in DH probabilities at the northern and southern ends of the island that are very similar to current conditions, indicating a high probability that DH < 3 m will continue into the future. Regions where DH currently exceeds 3 m (i.e., $P(\mathrm{DH} < 3\ \mathrm{m})$ is low; mapped in blue in Figure 12a) are predicted to be less likely under the increased erosion scenarios. Under scenario 3 (most extreme erosion), $P(\mathrm{DH} < 3\ \mathrm{m})$ is between 0.33 and 0.5 along much of the island and low dunes are "about as likely as not" when considered in terms of the Intergovernmental

Panel on Climate Change (IPCC) likelihood terminology [*Cubasch et al*., 2013] that is common in decision-making. This phrasing acknowledges increasing predictive uncertainty for scenarios that are approaching (but have not exceeded) conditions at the limit of our historical experience. This is not a prediction failure, as this result is different from the predictions under the current or more benign scenarios that include higher confidence: low dunes are predicted to be unlikely and extremely unlikely in the light and dark blue areas in Figure 12a. From a decision support perspective, knowing where dunes are very likely to be low (the ends of the island, unless the SLC rate becomes zero) and where one cannot rule out the possibility that they could be low (almost everywhere else) are both useful predictions.

The BN utilizes SLC, a valuable metric, which is derived for many coastlines [e.g., *USGS*, 2013] and depends on sea level rise among other factors [*Gutierrez et al*., 2011]. BNs such as that in *Gutierrez et al*. [2011] predict probabilities of shoreline changes at coarse (1–5 km) spatial resolution and long (100 year) timescales. The BN presented in this paper provides probabilities of geomorphic states at relatively high spatial resolution (analysis at 50 m alongshore resolution) and resolves short-scale features (DH, BW, and BH) that control storm vulnerability and define habitat suitability and extent relevant to land and species management goals. The forecasting scenario approach can be applied to management decisions affecting infrastructure vulnerability or maintenance of specific habitat characteristics over years to decades where response to specific storm events and sea level changes are uncertain and must be treated probabilistically. Because we include anthropogenic modifications in our analysis, our approach supports decisions relating to both reactive responses to climate and storm-driven processes (e.g., beach nourishment as a response to increased erosion) as well as proactive decisions to alter natural processes (e.g., optimizing habitat availability by allowing or promoting certain types of natural landscape change such as dune erosion and overwash).

6. Conclusions

This study demonstrates an approach to skillfully predict probabilities of specific barrier island geomorphic characteristics using Bayesian networks. We show that there are distinct geomorphic conditions associated with long-term shoreline change trends. Specifically, where shoreline change rates are erosional (SLC < -1 m/yr), the barrier island tends to be narrow, has lower dunes, and this setting occurs close to tidal inlets. In contrast, where shoreline change rates are accretional (SLC > 1 m/yr), the barrier island tends to be wider, has higher dunes, and this occurs farther away from tidal inlets. Where shoreline change rates are relatively stable (-1 m/yr $<$ SLC < 1 m/yr), barrier island morphology displays a wider range of variability. We find that the lowest prediction error rates are 28–38% and result for scenarios where the geomorphic outputs (DH, BW, or BH) are forecast independently. When DH, BW, and BH are forecast simultaneously, the error rates are higher (45–59%). Examination of the relative influence of the variables included in this BN shows that decadal- to centennial-scale attributes of the barrier island (i.e., SLC and AM) individually contribute most to skillful predictive performance. Skill is improved with the addition of DI, and more detailed variables (DH, BW, and BH) are important additions to maximize hindcast accuracy and improve BN skill when combined with the other variables. The eight-variable model's robustness was rigorously evaluated using data sets that spanned 50 km of coastline and three points in time. The mechanics of our BN framework were tested with a rigorous *k*-fold approach that identified the degree of overfitting (about 50% for the error rate) and showed that our primary BN had a justifiable level of complexity and that overfitting was minimized by using all available data. These conclusions were demonstrated via hindcast testing of seven possible training options for a single BN and an additional validation applied to the primary BN as well as to seven alternate models. Because the BN integrated data representing longer-term processes (e.g., shoreline change), short-term vulnerabilities (e.g., dune erosion), and anthropogenic modifications to the coast, it was used to predict future morphologic characteristics resulting from changes in large-scale behavior that has application to landscape and species management.

Acknowledgments

Funding for this work was provided by the U.S. Geological Survey (USGS) Coastal and Marine Geology Program and the U.S. Fish and Wildlife Service. We thank Anne Hecht of the U.S. Fish and Wildlife Service for providing the impetus for this study and for introducing us into the migratory shorebird research community. We thank Sarah Karpanty, Katy Gieder, Jim Fraser, and Dan Catlin of the Virginia Tech Department of Wildlife Conservation for their collaboration on this project. We thank Bill Hulslander, Jack Kumer, Tami Pearl, and Neil Winn of the National Park Service Assateague Island National Seashore for their willingness to provide access to the seashore and guidance regarding existing and data observations about the Assateague Island barrier island. We are also grateful to Dean Gesch and Jeff Danielson of the USGS EROS Data Center for their assistance in defining lidar elevation-based shorelines referenced to local tidal datums. We also appreciate assistance from Mike Fienen of the USGS Wisconsin Water Science Center who provided computer codes to implement model calibration and validation that is reported in the appendix. We thank Soupy Dalyander and Davina Passeri of the USGS, Evan Goldstein, Jesse McNinch, four anonymous reviewers, and the Editors for critical reviews of an earlier version of this manuscript. We thank JGR-ES Editor Giovanni Coco for his persistent and patient treatment of the revisions of this paper. The data used in this study are available from the U.S. Geological Survey as noted in section 3 as supporting information with this article, and the results reported here can be obtained from the first author. Any use of trade, firm, or product names is for descriptive purposes only and does not imply endorsement by the U.S. Government. Although these data have been processed successfully on a computer system at the U.S. Geological Survey (USGS), no warranty expressed or implied is made regarding the display or utility of the data on any other system or for general or scientific purposes, nor shall the act of distribution constitute any such warranty. The USGS or the U.S. Government shall not be held liable for improper or incorrect use of the data described and/or contained herein.

References

Bonisteel, J. M., A. Nayegandhi, J. C. Brock, C. W. Wright, S. Stevens, X. Yates, and E. S. Klipp (2009), *EAARL Coastal-Topography-Assateague Island National Seashore, 2008: Bare Earth*, *U.S. Geol. Surv. Data Ser*., vol. 447. [Available at http://pubs.usgs.gov/ds/447/.]

Climate Change Science Program (2009), *Coastal Sensitivity to Sea-Level Rise: A Focus on the Mid-Atlantic Region*, *A Rep. by the U. S. Clim. Change Sci. Program and the Subcom. on Global Change Res*., 320 pp., U.S. Environmental Protection Agency, Washington D. C.

Charniak, E. (1991), Bayesian networks without tears, *AI Mag*., *12*(4), 50–63.

Claudino-Sales, V., P. Wang, and M. H. Horwitz (2008), Factors controlling the survival of coastal dunes during multiple hurricane impacts in 2004 and 2005: Santa Rosa barrier island, Florida, *Geomorphology*, *95*, 295–315.
Cohen, J. B., L. M. Houghton, and J. D. Fraser (2009), Nesting density and reproductive success of Piping Plovers in response to storm-and human-created habitat changes, *Wildl. Monogr.*, *173*, 1–24.
Cooper, G. E., and E. Herskovits (1992), A Bayesian method for the induction of probabilistic networks from data, *Mach. Learn.*, *9*, 309–347.
Cooper, M. J. P., M. D. Beevers, and M. Oppenheimer (2008), The potential impacts of sea level rise on the coastal region of New Jersey, USA, *Clim. Change*, *90*, 475–492.
Corbella, S., and D. D. Stretch (2012), Predicting coastal erosion trends using non-stationary statistics and process-based models, *Coastal Eng.*, *70*, 40–49.
Cowell, P. J., P. S. Roy, and R. A. Jones (1995), Simulation of large-scale coastal change using a morphological behavior model, *Mar. Geol.*, *126*, 45–61, doi:10.1016/00253227(95)00065-7.
Cowell, P. J., B. G. Thom, R. A. Jones, C. H. Everts, and D. Simanovic (2006), Management of uncertainty in predicting climate-change impact on beaches, *J. Coast. Res.*, *22*(1), 232–245.
Cubasch, U., D. Wuebbles, D. Chen, M. C. Facchini, D. Frame, N. Mahowald, and J.-G. Winther (2013), Introduction, in *Climate Change 2013: The Physical Science Basis. Contribution of Working Group I to the Fifth Assessment Report of the Intergovernmental Panel on Climate Change*, edited by T. F. Stocker et al., pp. 119–158, Cambridge Univ. Press, Cambridge, U. K., and New York.
Davis, R. A. (1994), Barrier island systems—A geologic overview, in *Geology of Holocene Barrier Island Systems*, edited by R. A. Davis Jr., pp. 1–46, Springer, New York.
Day, J. W., Jr., et al. (2007), Restoration of the Mississippi Delta: Lessons from hurricanes Katrina and Rita, *Science*, *315*, 1679–1684, doi:10.1126/science.1127030.
Dean, R. G., and M. Perlin (1977), A coastal engineering study of Ocean City inlet, in *CoastalSediments '77*, pp. 520–540, Am. Soc. of Civil Eng., Reston, Va.
Dolan, R., H. F. Lins, and J. Stewart (1980), Geographical analysis of Fenwick Island, Maryland, a middle Atlantic coast barrier island, *U.S. Geol. Surv. Prof. Pap.*, *1177-A*, 24 pp., U.S. Gov. Print. Off., Washington, D. C.
Doran, K. S., H. F. Stockdon, K. L. Sopkin, D. M. Thompson, and N. G. Plant (2012), National assessment of hurricane-induced coastal erosion hazards: Mid-Atlantic coast, *U.S. Geol. Surv. Open File Rep., 2013–1131*, p. 28.
Ells, K., and A. B. Murray (2012), Long-term, non-local coastline responses to local shoreline stabilization, *Geophys. Res. Lett.*, *39*, L19401, doi:10.1029/2012GL052627.
Fenster, M., and R. Dolan (1996), Assessing the impact of tidal inlets on adjacent barrier island shorelines, *J. Coastal Res.*, *12*(1), 294–310.
Fienen, M. N., and N. G. Plant (2015), A cross-validation package driving Netica with python, *Environ. Modell. Software*, *63*, 14–23, doi:10.1016/j.envsoft.2014.09.007.
FitzGerald, D. M., M. S. Fenster, B. Argow, and I. V. Buynevich (2008), Coastal impacts due to sea-level rise, *Annu. Rev. Earth Planet. Sci.*, *36*, 601–647, doi:10.1146/annurev.earth.35.031306.140139.
Gesch, D. B., B. T. Gutierrez, and S. K. Gill (2009), Coastal elevations, in *Coastal Sensitivity to Sea-Level Rise: A Focus on the Mid-Atlantic Region*, pp. 25–42, U.S. Clim. Change Sci. Program, Washington, D. C.
Gieder, K. D., S. M. Karpanty, J. D. Fraser, D. H. Catlin, B. T. Gutierrez, N. G. Plant, A. M. Turecek, and E. R. Thieler (2014), A Bayesian network approach to prediction nest presence of the federally-threatened piping plover (*Charadrius melodus*) using barrier island features, *Ecol. Modell.*, *276*, 38–50.
Gutierrez, B. T., S. J. Williams, and E. R. Thieler (2007), Potential for shoreline changes due to sea-level rise along the U.S. Mid-Atlantic region, *U.S. Geol. Surv. Open File Rep., 2007–1278*, p. 34. [Available at http://woodshole.er.usgs.gov/pubs/of2007-1278/.]
Gutierrez, B. T., S. J. Williams, and E. R. Thieler (2009), Ocean coasts, in *Coastal Sensitivity to Sea-Level Rise: A Focus on the Mid-Atlantic Region*, pp. 43–56, U. S. Clim. Change Sci. Program, Washington, D. C.
Gutierrez, B. T., N. G. Plant, and E. R. Thieler (2011), A Bayesian network to predict coastal vulnerability to sea level rise, *J. Geophys. Res.*, *116*, F02009, doi:10.1029/2010JF001891.
Hapke, C., and N. G. Plant (2010), Predicting coastal cliff erosion using a Bayesian probabilistic model, *Mar. Geol.*, *278*, 140–149.
Hapke, C., E. Himmelstoss, M. Kratzmann, J. List, and E. Thieler (2011), National assessment of shoreline change: Historical shoreline change along the New England and Mid-Atlantic coasts, *U.S. Geol. Surv. Open File Rep., 2010–1118*. [Available at http://pubs.usgs.gov/of/2010/1118/.]
Hapke, C. J., M. G. Kratzmann, and E. A. Himmelstoss (2013), Geomorphic and human influence on large-scale coastal change, *Geomorphology*, *199*, 160–170, doi:10.1016/j.geomorph.2012.11.025.
Hayes, M. O. (1979), Barrier island morphology as a function of tidal and wave regime, in *Barrier Islands from the Gulf of St. Lawrence to the Gulf of Mexico*, edited by S. P. Leatherman, pp. 1–27, Academic Press, New York.
Himmelstoss, E., M. Kratzmann, C. Hapke, E. Thieler, and J. List (2010), The national assessment of shoreline change: A GIS compilation of vector shorelines and associated shoreline change data for the New England and mid-Atlantic coasts, *U.S. Geol. Surv. Open File Rep., 2010–1119*. [Available at http://pubs.usgs.gov/of/2010/1119/.]
Jensen, F. V., and T. D. Nielsen (2007), *Bayesian Networks and Decision Graphs*, Springer, New York.
Kirshen, P., K. Knee, and M. Ruth (2008), Climate change and coastal flooding in Metro Boston: Impacts and adaptation strategies, *Clim. Change*, *90*, 453–473.
Krantz, D. K., C. A. Schupp, C. C. Spaur, J. E. Thomas, and D. V. Wells (2009), Dynamic systems at the land-sea interface, in *Shifting Sands: Environmental and Cultural Change in Maryland's Coastal Bays*, edited by W. C. Dennison et al., pp. 193–230, IAN Press at Univ. of Maryland Center for Environ. Sci., Cambridge, Md.
Lauritzen, S. L. (1995), The EM algorithm for graphical association models with missing data, *Comput. Stat. Data Anal.*, *19*, 191–201.
Leatherman, S. P. (1983), Barrier dynamics and landward migrate with Holocene sea-level rise, *Nature*, *301*(3), 415–417.
Lentz, E., and C. J. Hapke (2011), *The Development of a Probabilistic Approach to Forecast Shoreline Change*, *Proc. Coast. Seds.*, vol. 11, pp. 1853–1866, Amer. Soc. Civ. Eng., Reston, Va, and Miami, Fla.
Lindemer, C. A., N. G. Plant, J. A. Puleo, D. M. Thompson, and T. V. Wamsley (2010), Numerical simulation of a low-lying barrier island's morphological response to Hurricane Katrina, *Coastal Eng.*, *57*, 985–995, doi:10.1016/j.coastaleng.2010.06.004.
List, J. H., A. S. Farris, and C. Sullivan (2006), Reversing storm hotspots on sandy beaches: Spatial and temporal characteristics, *Mar. Geol.*, *226*(3–4), 261–279.
Loegering, J. P., and J. D. Fraser (1995), Factors affecting piping plover chick survival in different brood rearing habitats, *J. Wildl. Manage.*, *59*(4), 646–655.

Lorenzo-Trueba, J., and A. D. Ashton (2014), Rollover, drowning, and discontinuous retreat: Distinct modes of barrier response to sea-level rise arising from a simple morphodynamic model, *J. Geophys. Res. Earth Surface*, *119*, 779–801, doi:10.1002/2013JF002941.

Magliocca, N. R., D. E. McNamera, and A. B. Murray (2011), Long-term large-scale morphodynamic effects of artificial dune construction along a barrier island coastline, *J. Coastal Res.*, *27*(5), 918–930.

Marcot, B. G., J. D. Steventon, G. D. Sutherland, and R. K. McCann (2006), Guidelines for developing and updating Bayesian belief networks applied to ecological modeling and conservation, *Can. J. For. Res.*, *36*, 3063–3074.

Masterson, J. P., M. N. Fienen, E. R. Thieler, D. B. Gesch, B. T. Gutierrez, and N. G. Plant (2013), Effects of sea-level rise on barrier island groundwater system dynamics-ecohydrological implications, *Ecohydrology*, doi:10.1002/eco.1442.

McCall, R. T., J. S. M. Van Thiel de Vries, N. G. Plant, A. R. Van Dongeren, J. A. Roelvink, D. M. Thompson, and A. J. H. M. Reniers (2010), Two-dimensional time dependent hurricane overwash and erosion modeling at Santa Rosa Island, *Coastal Eng.*, *57*, 668–683, doi:10.1016/j.coastaleng.2010.02.006.

McNamara, D. E., and B. T. Werner (2008a), Coupled barrier island–resort model: 1. Emergent instabilities induced by strong human-landscape interactions, *J. Geophys. Res.*, *113*, F01016, doi:10.1029/2007JF000840.

McNamara, D. E., and B. T. Werner (2008b), Coupled barrier island-resort model: 2. Tests and predictions along ocean city and Assateague Island National Seashore, Maryland, *J. Geophys. Res.*, *113*, F01017, doi:10.1029/2007JF000841.

McNamara, D. E., A. B. Murray, and M. D. Smith (2011), Coastal sustainability depends on how economic and coastline responses to climate change affect each other, *Geophys. Res. Lett.*, *38*, L07401, doi:10.1029/2011GL047207.

Melillo, J. M., T. C. Richmond, and G. W. Yohe (Eds.) (2014), Climate change impacts in the United States: The third national climate assessment, U.S. Global Change Research Program, 841 pp., doi:10.7930/J0Z31WJ2.

Moore, L. J., J. H. List, S. J. Williams, and D. Stolper (2010), Complexities in barrier island response to sea-level rise: Insights from numerical model experiments, North Carolina, Outer Banks, *J. Geophys. Res.*, *115*, F03004, doi:10.1029/2009JF001299.

Morton, R. A., and T. L. Miller (2005), National assessment of shoreline change: Part 2. Historical shoreline changes and associated land loss along the U.S. Southeast Atlantic Coast, U.S. Geol. Surv. Open File Rep., 2005–1401. [Available at http://pubs.usgs.gov/of/2005/1401/.]

Morton, R. A., and A. H. Sallenger Jr. (2003), Morphological impacts of extreme storms on sandy beaches and barriers, *J. Coastal Res.*, *19*(3), 560–573.

Morton, R. A., J. G. Paine, and J. C. Gibeaut (1994), Stages and durations of post-storm beach recovery, southeastern Texas, coast USA, *J. Coastal Res.*, *10*(4), 884–908.

Morton, R. A., T. L. Miller, and L. J. Moore (2004), National assessment of shoreline change: Part 1. Historical shoreline changes and associated land loss along the U.S. Gulf of Mexico, *U.S. Geol. Surv. Open File Rep., 2004–1043*. [Available at http://pubs.usgs.gov/of/2004/1043/.]

Morton, R. A., J. E. Bracone, and B. Cooke (2007), Geomorphology and depositional sub environments of Assateague Island MD/VA, *U.S. Geol. Surv. Open File Rep., 2007–1388*. [Available at http://pubs.usgs.gov/of/2007/1388/.]

Moslow, T. F., and S. D. Heron Jr. (1994), The Outer Banks of North Carolina, in *Geology of Holocene Barrier Island Systems*, edited by R. A. Davis Jr., pp. 47–74, Springer, New York.

Najjar, R. G., et al. (2000), The potential impacts of climate change on the mid-Atlantic coastal region, *Clim. Res.*, *14*, 219–233, doi:10.3354/cr014219.

NOAA (2009), Nor-Ida. [Available at www.stormsurge.noaa.gov/event_history.html, (accessed 4/29/2013).]

NOAA (2011), Hurricane Irene. [Available at http://www.stormsurge.noaa.gov/event_history_2010s.html, (accessed 4/29/2013).]

Nordstrom, K. F. (1988), Effects of shore protection and dredging projects on beach configuration near tidal inlets in New Jersey, in *Hydrodynamics and Sediment Dynamics of Tidal Inlets*, edited by D. G. Aubrey and L. Weishar, pp. 440–454, Springer, New York.

National Ocean Service (2011), NOAA National Ocean Service Tides and Currents Online: Tidal station datums. [Available at http://tidesandcurrents.noaa.gov/datums.html?id=8570280, (Accessed 3/14/2011).]

Passeri, D. L., S. C. Hagen, S. C. Medeiros, M. V. Bilskie, K. Alizad, and D. Wang (2015), The dynamic effects of sea level rise on low-gradient coastal landscapes: A review, *Earth's Future*, doi:10.1002/2015EF000298.

Plant, N. G., and K. T. Holland (2011), Prediction and assimilation of surf-zone process using a Bayesian network. Part I: Forward models, *Coast. Eng.*, *58*, 119–130, doi:10.1016/j.coasteng.2010.09.003.

Plant, N. G., and H. F. Stockdon (2012), Probabilistic prediction of barrier-island response to hurricanes, *J. Geophys. Res.*, *117*, F03015, doi:10.1029/2011JF002326.

Plant, N. G., H. F. Stockdon, J. Flocks, A. H. Sallenger, J. W. Long, J. M. Cormier, K. Guy, and D. M. Thompson (2012), Prediction of barrier island restoration response and its interactions with the natural environment, paper presented at AGU Fall Meeting, 3–7 Dec., San Francisco, Calif.

Plant, N. G., J. Flocks, H. F. Stockdon, J. W. Long, K. Guy, D. M. Thompson, J. M. Cormier, C. G. Smith, J. L. Miselis, and P. S. Dalyander (2014), Predictions of barrier island berm evolution in a time-varying storm climatology, *J. Geophys. Res. Earth Surface*, *119*, 300–316, doi:10.1002/2013JF002871.

Roelvink, J. A., A. Reniers, A. van Dongeren, J. van Thiel de Vries, R. McCall, and J. Lescinski (2009), Modeling storm impacts on beaches, dunes and barrier islands, *Coast. Eng.*, *56*, 1133–1152.

Romine, B. M., C. H. Fletcher, M. M. Barbee, T. R. Anderson, and L. N. Frazer (2013), Are beach erosion rates and sea-level rise related in Hawaii?, *Global Planet. Change*, *108*, 149–157.

Sallenger, A. H., Jr. (2000), Storm impact scale for barrier islands, *J. Coastal Res.*, *16*(3), 890–895.

Schupp, C. A., N. T. Winn, T. L. Pearl, J. P. Kumer, T. J. B. Caruthers, and C. S. Zimmerman (2013), Restoration of overwash processes creates piping plover (*Charadrius melodus*) habitat on a barrier island (Assateague Island, Maryland), *Estuarine Coastal Shelf Sci.*, *116*, 11–20.

Sherwood, C. R., J. W. Long, P. J. Dickhudt, P. S. Dalyander, D. M. Thompson, and N. G. Plant (2014), Inundation of a barrier island (Chandeleur Islands, Louisiana, USA) during a hurricane: Observed water-level gradients and modeled seaward sand transport, *J. Geophys. Res. Earth Surface*, *119*, 1498–1515, doi:10.1002/2013JF003069.

Slott, J. M., A. B. Murray, and A. D. Ashton (2010), Large-scale responses of complex-shaped coastlines to local shoreline stabilization and climate change, *J. Geophys. Res.*, *115*, F03033, doi:10.1029/2009JF001486.

Stockdon, H. F., A. H. Sallenger, R. A. Holman, and P. A. Howd (2007), A simple model for the spatially-variable coastal response to hurricanes, *Mar. Geol.*, *238*, 1–20.

Stockdon, H. F., K. S. Doran, and A. H. Sallenger Jr. (2009), Extraction of lidar-based dune-crest elevations for use in examining the vulnerability of beaches to inundation during hurricanes, *J. Coastal Res.*, *53*, 59–65, doi:10.2112/SI53-007.1.

Stockdon, H. F., K. J. Doran, D. M. Thompson, K. L. Sopkin, N. G. Plant, and A. H. Sallenger (2012), National assessment of hurricane-induced coastal erosion hazards: Gulf of Mexico, *U.S. Geol. Surv. Open File Rep., 2012–1084*, 51 pp.

Stolper, D., J. H. List, and E. R. Thieler (2005), Simulating the evolution of coastal morphology and stratigraphy with a new morphological-behavior model (GEOMBEST), *Mar. Geol.*, *218*, 17–36, doi:10.1016/j.margeo.2005.02.019.

Stone, G. W., and R. A. McBride (1998), Louisiana barrier islands and their importance in wetland protection: Forecasting shoreline change and subsequent response of wave climate, *J. Coastal Res.*, *14*(3), 900–915.
Stone, G. W., X. Zhang, and A. Sheremet (2005), The role of barrier islands, muddy shelf, and reefs in mitigating the wave field along coastal Louisiana, *J. Coastal Res.*, *SI*(44), 40–55.
Strauss, B. H., R. Ziemlinski, J. L. Weiss, and J. T. Overpeck (2012), Tidally adjusted estimates of topographic vulnerability to sea level rise and flooding for the contiguous United States, *Environ. Res. Lett.*, *7*, 021001, doi:10.1088/1748-9326/7/1/014033.
Stutz, M. L., and O. H. Pilkey (2011), Open-ocean barrier islands: Global influence of climatic, oceanographic, and depositional settings, *J. Coastal Res.*, *27*(2), 207–222.
Thieler, E. R., and R. S. Young (1991), Quantitative evaluation of coastal geomorphological changes in South Carolina after Hurricane Hugo, *J. Coastal Res.*, *8*, 187–200.
Titus, J. G., and C. Richman (2001), Maps of lands vulnerable to sea level rise: Modeled elevations along the US Atlantic and Gulf coasts, *Clim. Res.*, *18*, 205–228, doi:10.3354/cr018205.
Tribbia, J., and S. C. Moser (2008), More than information: What coastal managers need to plan for climate change, *Environ. Sci. Policy*, *11*, 315–328.
Truitt, R. V. (1968), *High Winds….High Tides: A Chronicle of Maryland's Coastal Hurricanes*, *Nat. Resour. Inst., Educational Ser.*, vol. 77, 35 pp., Univ. of Maryland, College Park, Md.
U.S. Geological Survey (USGS) (2009), Coastal change hazards: Hurricanes and extreme storms, Nor'Ida. [Available at http://coastal.er.usgs.gov/hurricanes/norida, (accessed 4/29/2013).]
U.S. Geological Survey (USGS) (2011), Coastal change hazards: Hurricanes and extreme storms, Hurricane Irene. [Available at http://coastal.er.usgs.gov/hurricanes/irene, (accessed 4/29/2013).]
U.S. Geological Survey (USGS) (2012), Coastal change hazards: Hurricanes and extreme storms, Hurricane Sandy. [Available at http://coastal.er.usgs.gov/hurricanes/sandy, (accessed 4/29/2013).]
U.S. Geological Survey (USGS) (2013), National Assessment of Shoreline Change Project. [Available at http://coastal.er.usgs.gov/shoreline-change/, (accessed 6/10/2013).]
van den Hoek, R. E., M. Brugnach, and A. Y. Hoekstra (2012), Shifting to ecological engineering in flood management: Introducing new uncertainties in the development of a building with nature pilot project, *Environ. Sci. Policy*, *22*, 85–99.
Weber, K. M., J. H. List, and K. L. M. Morgan (2005), An operational mean high water datum for determination of shoreline position from topographic lidar data, *U.S. Geol. Surv. Open File Rep., 2005–1027*. [Available at http://pubs.usgs.gov/of/2005/1027/.]
Weigend, A. S., and R. J. Bahnsali (1994), Paradigm change in prediction, *Phil. Trans. Phys. Sci. Eng.*, *348*(1688), 405–418.
Weiss, J. L., J. T. Overpeck, and B. Strauss (2011), Implications of recent sea level rise science for low-elevation areas in coastal cities of the conterminous U.S.A.: A letter, *Clim. Change*, *105*, 635–645.
Wikle, C. K., and L. M. Berliner (2007), A Bayesian tutorial for data assimilation, *Phys. D*, *230*, 1–16.
Yang, Z., E. Myers, A. Wong, and S. White (2008), VDatum for Chesapeake Bay, Delaware Bay and adjacent coastal water areas: Tidal datums and sea surface topography, NOAA Technical Report NOS CS 15, p. 110, National Oceanic and Atmospheric Administration, U.S. Department of Commerce.
Zhang, K., B. C. Douglas, and S. P. Leatherman (2002), Do storms cause long-term beach erosion along the U.S. east barrier coast?, *J. Geol.*, *110*(4), 493–502.